AD-A055 772 PANAMETRICS INC WALTHAM MASS F/G 4/1
STRATCOM VI-A UV FLUX AND 30-65 KM LOW-BACKGROUND BETASONDE AIR--ETC(U)
JUL 76 B SELLERS, F A HANSER, J L HUNERWADEL DAAD07-75-C-0124
UNCLASSIFIED PANA-AIR-1 NL

1 OF 1
ADA
055772

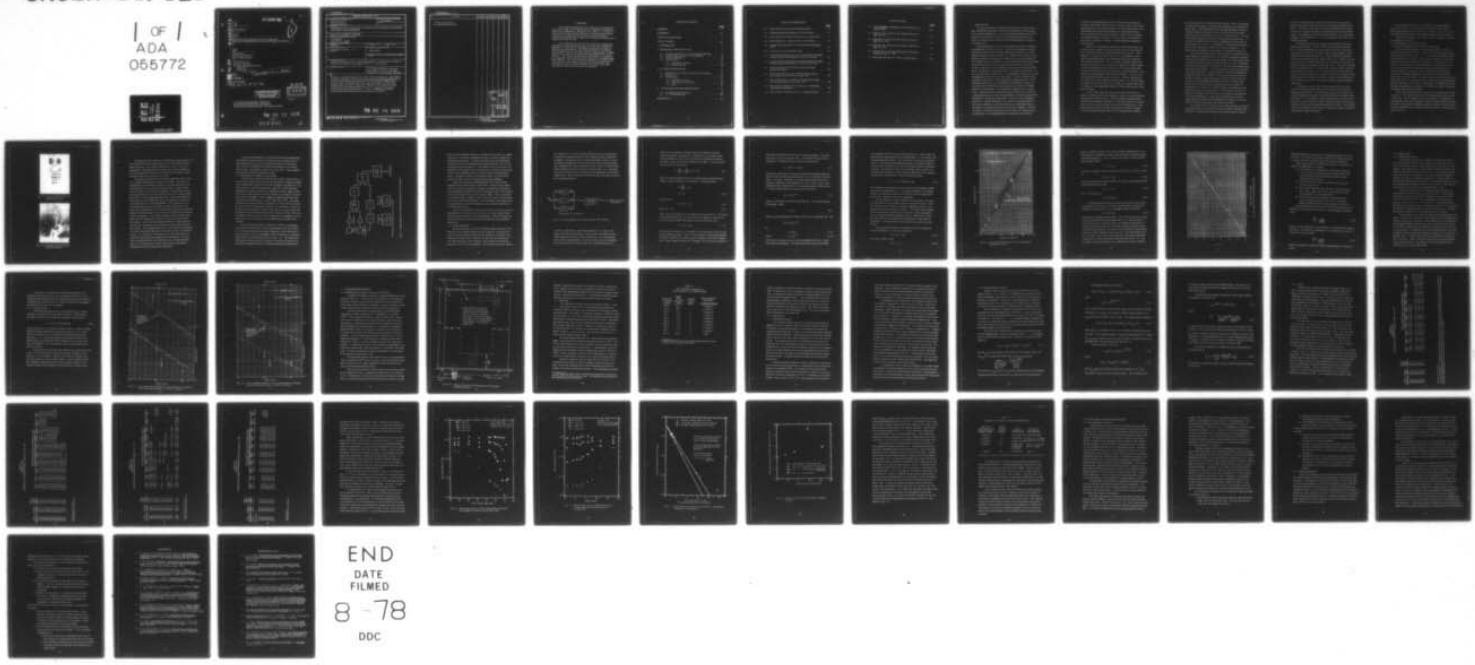

END
DATE
FILMED
8-78
DDC

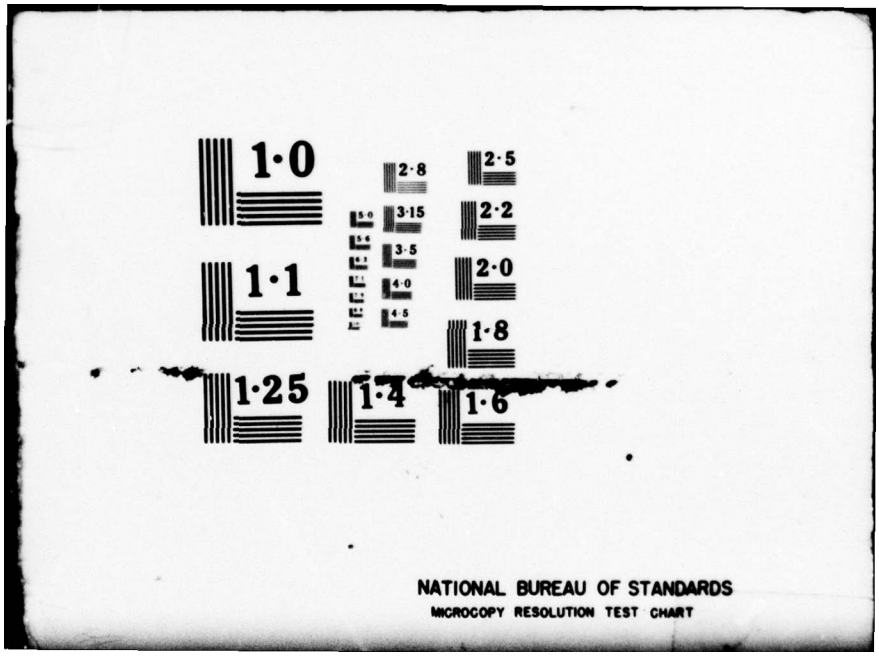
1·0
1·1
1·25
1·4
1·6
1·8
2·0
2·2
2·5
2·8
3·15
3·5
4·0
4·5
NATIONAL BUREAU OF STANDARDS
MICROCOPY RESOLUTION TEST CHART

FOR FURTHER TRAN

(14) PANA-AIR-1

(6) STRATCOM VI-A UV FLUX AND 30-65 KM LOW-BACKGROUND BETASONDE AIR DENSITY MEASUREMENTS.

(10) Bach/Sellers, Frederick A./Hanser Jean L./Hunerwadel

Panametrics, Inc.
221 Crescent Street
Waltham, Massachusetts 02154

(12) 57p.

(15) DAAD07-75-C-0124

(11) July 1976

(9) Final Report.
11 Jul 75-31 Jul 76

U.S. ARMY ELECTRONICS COMMAND
ATMOSPHERIC SCIENCES LABORATORY
WHITE SANDS MISSILE RANGE, NEW MEXICO 88002

Unclassified

Security Classification

DOCUMENT CONTROL DATA - R & D

(Security classification of title, body of abstract and indexing annotation must be entered when the overall report is classified)

1. ORIGINATING ACTIVITY *(Corporate author)*
Panametrics, Inc.
221 Crescent St.
Waltham MA 02154

2a. REPORT SECURITY CLASSIFICATION
Unclassified

2b. GROUP

3. REPORT TITLE
STRATCOM VI-A UV FLUX AND 30-65 KM LOW-BACKGROUND BETASONDE AIR DENSITY MEASUREMENTS

4. DESCRIPTIVE NOTES *(Type of report and inclusive dates)*
Final, 11 July 1975 - 31 July 1976

5. AUTHOR(S) *(First name, middle initial, last name)*
Bach Sellers
Frederick A. Hanser
Jean L. Hunerwadel

6. REPORT DATE
July 1976

7a. TOTAL NO. OF PAGES
57

7b. NO. OF REFS
21

8a. CONTRACT OR GRANT NO.
DAAD07-75-C-0124

b. PROJECT NO.

c.

d.

9a. ORIGINATOR'S REPORT NUMBER(S)
PANA-AIR-1

9b. OTHER REPORT NO(S) *(Any other numbers that may be assigned this report)*

10. DISTRIBUTION STATEMENT
Approved for public release, distribution unlimited. Reproduction in whole or in part is permitted for any purpose of the U. S. Government.

11. SUPPLEMENTARY NOTES

12. SPONSORING MILITARY ACTIVITY
U. S. Army Electronics Command
Atmospheric Sciences Laboratory
White Sands Missile Range, NM 88002

13. ABSTRACT

By use of a modified version of the CIAP UV Spectrophotometer, the altitude variation of 200-400 nm flux has been measured up to about 126 kft during the Stratcom (Stratospheric Composition) VI-A balloon flight at White Sands Missile Range, NM. Solar cycle associated variability of the flux in the important 220 nm region is discussed. Results are also given for direct measurement of air density in the 30-65 km region by use of an Arcas-mounted low-background Betasonde. Recommendations for obtaining further flight data with these two instruments are provided.

78 06 29 055

DD FORM 1 NOV 1473 REPLACES DD FORM 1473, 1 JAN 64, WHICH IS OBSOLETE FOR ARMY USE.

Unclassified

Security Classification

14. KEY WORDS	LINK A		LINK B		LINK C	
	ROLE	WT	ROLE	WT	ROLE	WT
UV flux measurement Air density measurement						

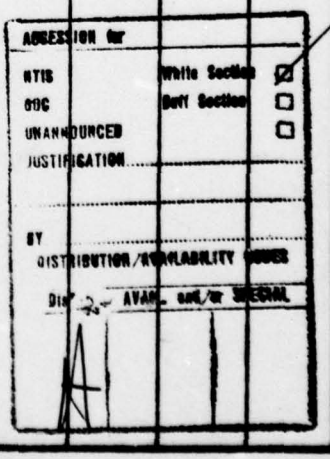

FOREWORD

The UV Spectrophotometer used in this work was fabricated for use in the Dept. of Transportation's Atmospheric Monitoring and Experiments Subprogram, managed by Mr. Samuel C. Coroniti, a major element of the Climatic Impact Assessment Program (CIAP). Funding was accomplished thru the Office of Naval Research. Design and fabrication of the original Low-background Betasonde was supported directly by ONR.

The modification and flight of the UVS and Low-background Betasonde, as reported herein, was carried out under Contract No. DAAD07-75-C-0124 with the Atmospheric Sciences Laboratory of White Sands Missile Range. The Contracting Officer's Technical Representative was Mr. Harold N. Ballard, whose guidance throughout the course of this work contributed significantly to the success achieved. The UVS was integrated into the Stratcom VI-A payload as a cooperative effort between Sandia Laboratories and White Sands Missile Range. The Low-background Betasonde was installed in the Arcas payload by Mr. Miguel Izquierdo and his associates of the University of Texas at El Paso (UTEP). Much of the basic data retrieval was also carried out by the UTEP group.

TABLE OF CONTENTS

LIST OF ILLUSTRATIONS

LIST OF TABLES

1. INTRODUCTION

The upper atmosphere analytical instrumentation which was flown under USAECOM sponsorship consists of an atmospheric density gauge and a UV Spectrophotometer. The density gauge was flown on an Arcas meteorological sounding rocket whereas the Spectrophotometer was flown on a balloon-borne scientific instrumentation payload, identified as Stratcom VI-A.

The density gauge is based on the principle of forward scattering and attentuation of beta-rays in air. An early version Betasonde incorporated 10 standard Geiger-Mueller (GM) tubes arranged in a circular pattern to detect the beta-rays (Ref. 1.1). Flight results in 1967 showed that the sensitivity of this gauge was limited by cosmic ray background in the 60 km region, and that above ~25 km the Betasonde-derived density exceeded that derived from temperature and pressure by as much as 40-50%. Summaries of work with the various versions of this type Betasonde - all using the standard GM tubes - have been presented (Ref. 1.2 - 1.4), and will not be repeated here. It is important to note however, that investigations of the cosmic ray effect (Ref. 1.3 and 1.4) confirmed the original assertion (Ref. 1.1) that although this background does, in fact, ultimately limit the accuracy obtainable at high altitudes, it does not account for the 40-50% error observed above 25 km in the 1967 flight. Rather it is the fact that vacuum calibration chambers can, in some cases, contain much larger fractions of water vapor than is present at a comparable pressure level in the atmosphere. When this is measured and properly taken into account (Refs. 1.4 and 1.5) in the calibration procedure, a density calibration curve will be obtained that applies to all pressure altitudes at which the difference in composition between atmosphere and calibration chamber is otherwise negligible. With the exception of variations introduced by water vapor, the composition of the atmosphere is essentially altitude-invariant up to about 100 km.

A similar situation probably prevails in most vacuum chambers at pressures above those requiring use of a diffusion pump or other type pump that could, by its pumping action, cause the composition to vary significantly from that in the atmosphere at comparable pressure. Thus, provided the water vapor fraction is measured in the chamber, it should be possible to calibrate down to pressures equivalent to at least 80 km - perhaps even higher - without additional composition measurements.

Thus, in all subsequent work the water vapor fraction has been measured in the chamber and the calibration procedure described in Ref. 1.4 has been followed, eliminating that source of error. Additionally, the cosmic ray effect has been very substantially reduced with design and fabrication under ONR sponsorship of an improved low-background Betasonde. The new design essentially replaces the standard GM counters with a type that has very much smaller volume, so that the background is 10-20 times less. The beta detection efficiency is almost as good as the larger volume type flown before, since the betas are stopped just inside the window anyway. There is a significant problem with these tubes, however. Namely, the plateau is very short and it shifts slightly with temperature. At -60°C the shift is sufficient to cause the count rate to change very significantly unless the voltage is chosen just right initially (so that it still operates in the plateau region).

A sonde with 2 GM tubes of the above design was flown on a balloon in September 1970 from Palastine, Texas. Very good data was obtained up to the 10 km region. At the 30 km float altitude however, the operating temperature dropped to -70°C which produced erroneous data due to the excessive plateau shift at this low temperature. This phenomenon was discovered after the flight and examined carefully. It was found that the plateau shift versus temperature plot exhibits

an inversion point for one particular bias voltage. Thus, it is possible to minimize the change of countrate with temperature by selecting the proper bias. This information and the fact that the balloon sonde was already configured to fit into an Arcas nosecone led to the present effort to fly the density gauge on an Arcas sounding rocket. The work to accomplish this and the results of this flight are reported here. A general description and the necessary modifications of the sonde are given in Section 2.1 and 2.2, respectively. The calibration procedure and the final calibration results are presented in Section 2.3. The flight results including the reduced data are contained in Section 2.4.

The UV Spectrophotometer (UVS) was flown on the Stratcom VI-A balloon payload in September 1975. The UVS was originally developed to measure high altitude solar UV fluxes from an aircraft as part of the Climatic Impact Assessment Program (CIAP). As a result of possible environmental degradation due to the SST, the CIAP was initiated under DOT sponsorship in 1970. One of the primary concerns was possible reduction of total ozone, with consequent increases in biologically important ultraviolet (UV) radiation. Part of the CIAP programwas to develop an extensive upper atmosphere monitoring system (Ref. 1.6) based on use of the high altitude WB57F aircraft. Included in that system was an ultraviolet spectrophotometer (UVS) developed by Panametrics, Inc. (Ref. 1.7), which was flown successfully on many flights and returned much useful data. The structure of UV flux vs latitude and longitude was measured in much greater detail than had ever been possible before, and by use of the data (in the Hartley-Huggins bands) computer-based mathematical techniques were developed for deduction of the total ozone above the aircraft.

Use of the UVS on the Stratcom VI-A balloon flight gave measurements of the solar UV flux in the 200-400 nm region at altitudes up to 130,000 ft. Of particular interest are the measurements at 220 nm,

a window in the atmospheric transmission lying between the peak of the ozone absorption at 250 nm and the strong oxygen absorption below 180 nm. This wavelength region is extremely important for the photochemistry of the upper atmosphere, particularly the 50,000-150,000 ft. region. The photolysis of many important pollutants, the chlorofluoromethanes in particular (Ref. 1.8), is due primarily to the solar UV in this 220 nm window.

The altitude dependence of the 220 nm solar flux has been only poorly measured (Ref. 1.9, p 5). Balloon measurements reported in Ref. 1.10 are questionable because the reported absolute solar fluxes are a factor of 3 lower than all other reported measurements, including the UVS data from Stratcom VI-A. Higher altitude (175-225 kft) rocket measurements have been reported (Ref. 1.11). Satellite measurements of solar UV radiation show that for wavelengths less than 300 nm the sun becomes increasingly variable (Ref. 1.12). The 220 nm flux data obtained on Stratcom VI-A, combined with a number of other solar flux measurements (see Section 3. 3. 3), suggest that the 220 nm solar flux increases with increasing solar activity as measured by sunspot number. Measurement of the 220 nm solar flux as a function of both altitude and time in solar cycle is thus a very important part of upper atmosphere experiments.

The remaining nine solar UV flux measurements are used mostly to obtain information about the ozone layer and certain other photochemical reactions. The 280-330 nm region can be used to calculate the total ozone along the air path to the sun for very thin to very thick layers. The 330-400 nm measurements provide a check on UVS operation since the sun has a stable, well known output at these wavelengths, and they are not significantly affected by ozone. The UVS thus measures an important part of the solar spectrum, a part necessary to understand the upper atmosphere.

The operation of the UVS on the Stratcom VI-A balloon flight is described in Section 3. Modifications to the UVS necessary for the balloon flight are discussed in Section 3.1. Section 3.2 gives the necessary calibration information, while flight results are given in Section 3.3.

A summary of operation and results is given in Section 4, for both the Betasonde and the UVS.

2. BETASONDE - LOW BACKGROUND

2.1 General Description of Low Background Betasonde

The air density Betasonde is based on the detection of forward scattered beta rays by GM tubes. A detailed theoretical analysis of the general principle is given in Ref. 1.1. Since the low background version was intended to fly on a balloon, where long counting time is available, only two such tubes are utilized in this design. The GM counters convert the energy of the incident beta particles into voltage pulses which are screened and further conditioned by the associated electronics. Two data outputs are simultaneously available from the instrument. One is an auto-ranging logarithmic count ratemeter with a range of 2 decades (.1-1kc and 1-10kc). The other output represents the screened pulses after they have been processed by a dead time circuit which limits the pulse repetition rate to 2 kHz. This frequency limitation and the fact that both data outputs are clamped to +5V make these signals compatible with standard IRIG telemetry inputs.

Power for the electronics and the GM tubes is derived from DC/DC converters. They operate from the +28V on-board battery and consume a total of 2W. The HV supply for the Geiger counters is completely encapsulated for high vacuum operation. All low voltage electronic circuits are potted with a thermal insulating compound to reduce heat loss and to increase reliability under vibration and shock conditions. This is clearly shown in Fig. 2.1.

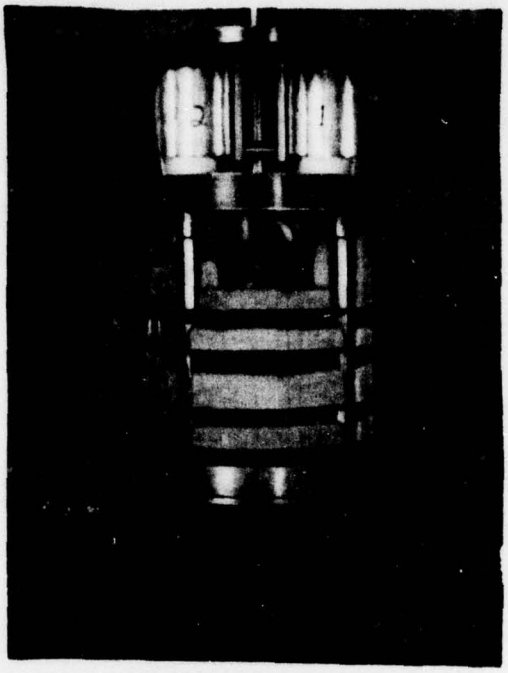

Fig. 2.1 Geiger-Mueller Tubes and Potted Electronics

Fig. 2.2 Complete Betasone Showing G-M Tube Windows

The physical configuration of the instrument is shown in Fig. 2. 2. Two cylinders with an overall length of 6-1/2" house the electronics and the GM tubes. The cylinder diameters are 4-1/4" and 3-1/2", respectively. Extending from the center of the smaller cylinder is a 12" boom which carries the annular beta source and source shield. The total weight of the instrument is 2. 8 lbs.

The sonde described above was flown in September 1970 as part of a scientific balloon payload, sponsored by ONR. The data were transmitted by an FM/FM transmitter to a ground station where the composite signal was recorded on magnetic tape. Analysis of the processed tape record showed the following. During ascent the data was in good agreement with the densities of the U. S. Standard Atmosphere (Ref. 2. 1) up to approximately 10 km. Above that altitude the count rate increased significantly above the standard values and remained high up to the 30 km float altitude. This behavior was not consistent with the known calibration and other system tests, and hence some post flight tests were carried out. The plateau versus bias voltage of the GM counters was remeasured and plotted with temperature as a parameter. This graph revealed an inversion point of the plateau over the temperature range of our tests for one particular bias voltage. At the inversion point the count rate change with temperature has a minimum, and it steadily increases with increasing bias voltage. Our preflight plateau tests were made at room temperature and the operating voltage was chosen in the center of the plateau at 560V. Our experience with larger volume GM tubes had not revealed the large temperature dependence of the plateau. Since the inversion point for these small GM tubes occurs at approximately 490V, it is evident why the density measurement on the balloon exhibited the observed temperature dependence.

The successful diagnosis of the problem thru the post flight tests described above encouraged the proposal for an air density measurement utilizing an Arcas rocket as the launch vehicle for this gauge. This could be accomplished with slight modifications of the existing density gauge, including the change of the HV to 490V. These modifications are described in the following section.

2.2 Modifications for Flight on Arcas Rocket

A block diagram of the modified sonde circuity is shown in Fig. 2.3. Based on the results of the balloon-borne instrument, the plateau voltage versus temperature characteristic of the GM tubes to be flown was carefully measured. Over the temperature range 0° to $+45^{\circ}$C both tubes exhibit their minimum temperature coefficient at a bias voltage of 491V. Thus, the sensing network for the HV regulator was changed to give precisely 491V at its output. The HV supply was temperature tested and showed no measurable change over the range 0° to $+45^{\circ}$C. The output countrate of the tubes deviates $\pm .6\%$ between $+5^{\circ}$ and $+40^{\circ}$C increasing to $\pm 1.5\%$ at the two temperature extremes. As described in a later section the actual temperature variation of the tubes was measured during the parachute descent and found to be only 5°C from $+25^{\circ}$ to $+30^{\circ}$C over the altitude range of interest. This corresponds to a negligible error in output countrate when compared to the statistical uncertaintly of the countrate.

Since the above temperature range (0° to $+45^{\circ}$C) is an estimate derived from measurements of other payloads flown on Arcas rockets, it is of interest to measure the actual temperature of the GM tubes for this instrument. This is accomplished with the addition of a small thermistor head in close proximity with one of the tubes. The signal from the thermistor is processed by a voltage to frequency converter (V/F) such that the output frequency is directly proportional to temperature.

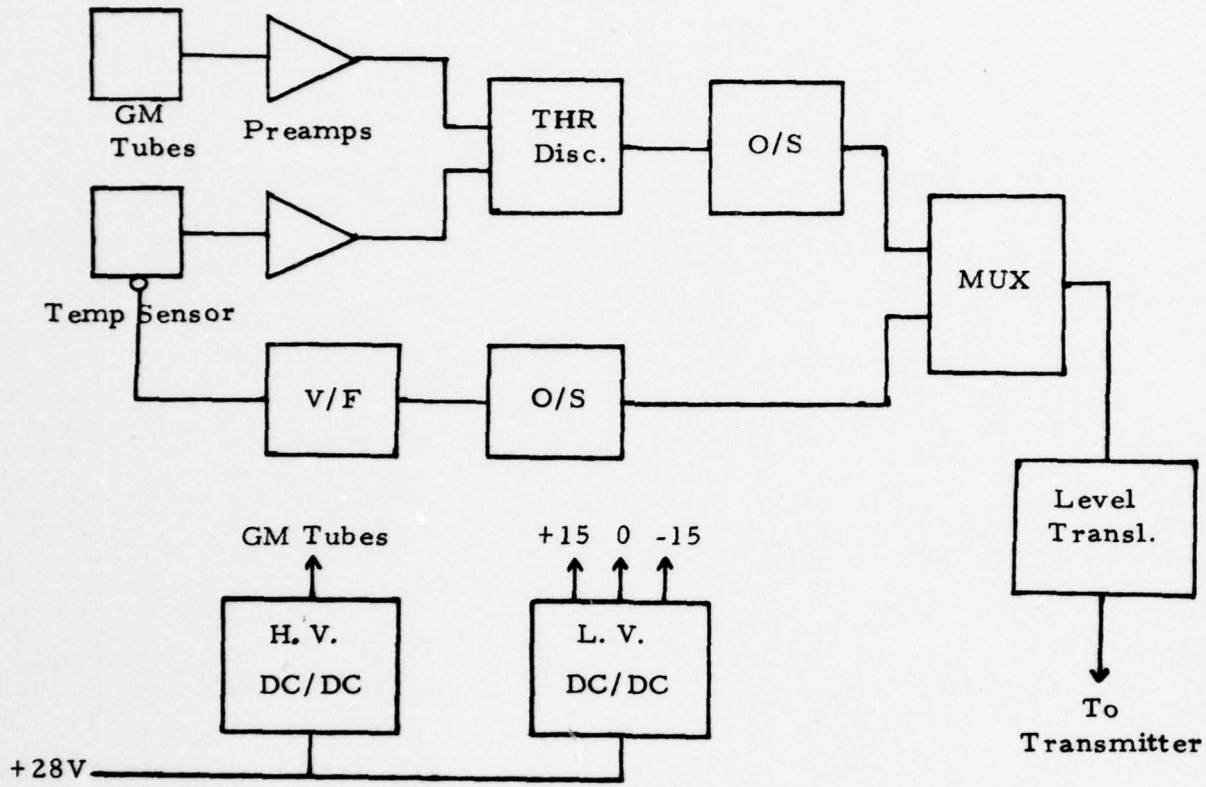

Fig. 2.3 Block Diagram of Modified Betasonde for Arcas Rocket.

Since only one telemetry channel is available on this rocket, the output from the V/F converter is multiplexed with the countrate output from the GM tube electronics. This time sharing process is proportioned to allow 45 sec. for the transmission of density data and 5 sec. for the temperature monitor frequency. The addition of the circuit board containing the V/F converter did not increase the overall size of the sonde because it was installed in place of the logarithmic count ratemeter board. The latter was flown on the balloon sonde, described in the previous section, because of increased telemetry capability.

On the Arcas the information bandwidth of the TM is 10k cps, sufficient for the expected pulse information. Because of the random nature of the pulses a frequency limiting circuit has to be introduced. Since the balloon sonde had the same requirement it was only necessary to decrease the dead-time of that circuit to 200μs. This is equivalent to a maximum pulse repetition rate of 5k cps and leaves enough margin never to exceed the TM bandwidth. The transmitter input requirement of negative pulses with a 12V amplitude was met with the addition of a level translator circuit.

In order to integrate the Betasonde with the Arcas power pack and transmitter it was only necessary to machine a simple adaptor plate, which attached to the power pack with standoffs. Input and Output connections to the sonde were hand wired to the battery and transmitter respectively.

2. 3 Density Calibration

As observed above, in order to limit the output count rate of the Betasonde to the maximum allowed by the telemetry, a dead-time circuit is used between the GM tubes and the telemetry (TM) input. This dead-time is on the order of 200μsec, and the GM tubes themselves also have dead-times which, although small compared to that of the dead-time circuit, are not negligible. The fact that the Pm-147 source

has a half-life of 2.6 years requires that source decay be taken into account if any significant period of time elapses between calibration and flight. The presence of the various dead-times, however, causes the Betasonde output not to be a linear function of the source intensity. This complicates the data reduction procedure, and one method of handling the problem has been discussed previously (Ref. 1.1). Basically, it involves deriving a source-decay corrected calibration curve for the output to TM. Here we present an alternative procedure that we believe to be somewhat simpler.

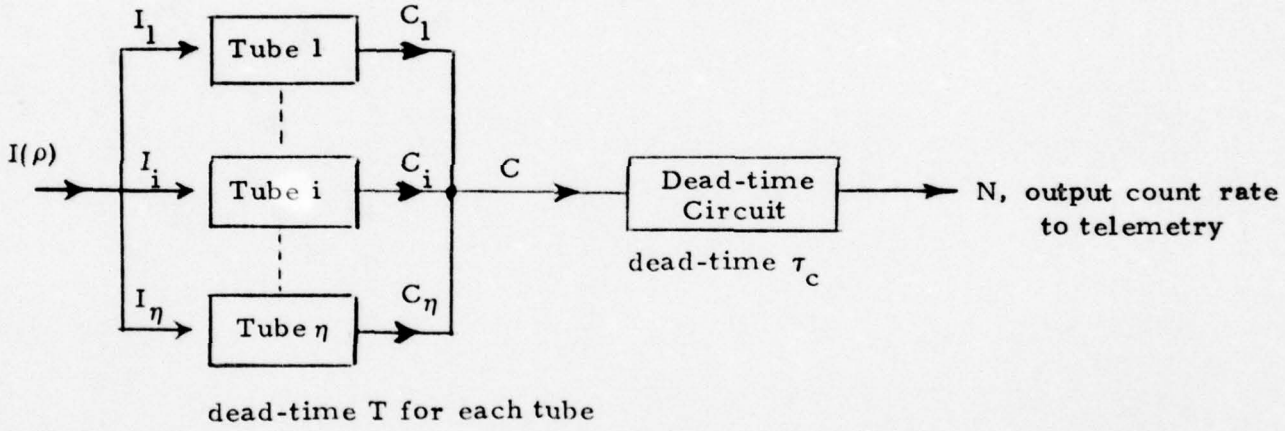

Fig. 2.4 Block Diagram for Analysis of Dead-Time Effects

An array of η GM tubes, each having dead-time T, is shown. The output count rates are labelled C_i, and the count rates that the tubes would experience if T were zero are labelled I_i. It is assumed that both C and N are measurable. Of course, the I_i are not measurable, but if the dead-time T is known they can be calculated from the C_i -

which can be measured if desired simply by blocking the interface window to all tubes except the i^{th}. In practice we are not interested in the individual I_i and C_i, but on the totals for all tubes acting simultaneously. Thus, by use of the standard result (Ref. 2.2) for the effect of a dead-time circuit we have

$$C = \sum_{i=1}^{\eta} C_i = \sum_{i=1}^{\eta} I_i/(1 + TI_i) \tag{2.1}$$

Now if it is assumed that the tubes are approximately equally efficient (which is easily verified by measuring the C_i individually) then

$$I = \sum_{i=1}^{\eta} I_i = \eta I_i$$

$$I_i = I/\eta \tag{2.2}$$

and from (2.1)

$$C = I/(1 + T_c I) \tag{2.3}$$

where $T_c = T/\eta$ (2.4)

Thus, the array of tubes acts as a single tube of dead-time T_c. Of course, at any particular time Eq. (2.3) may be taken to <u>define</u> a count rate I in terms of the measurable total output count rate of the GM array:

$$I = C/(1 - T_c C) \tag{2.5}$$

In that sense the choice of T_c is arbitrary; in the practical sense it is not, for the following reasons. First, at low density the scattering probability is linearly related to air density ρ because multiple scattering is unimportant. In this region the count rate I (but <u>not</u> C) is thus linearly related to ρ,

which can be directly checked from the calibration results. This will only occur if T_c has the proper value. For the EON Type 6213 tubes used here, T = 25 μsec and since 2 tubes were used ($\eta = 2$)

$$T_c = 25/2 = 12.5\ \mu\text{sec} \tag{2.6}$$

Because the count rates are low at low density the fractional difference between I and C is not large in this region, so C varies almost linearly with ρ. Secondly, I (but not C) is directly proportional to the source intensity, regardless of the dependence of I on ρ. Thus, if $I_o(\rho)$ is the calibration curve derived from (2.5) by measurements of $C_o(\rho)$ at time t = 0, then at any later time t the curve for $I(\rho)$ will be

$$I(\rho) = I_o(\rho)e^{-t/\tau} \tag{2.7}$$

where τ = 1378 days is the mean-life for Pm-147. For the high altitude, low-density, region

$$\rho = k_o I_o \tag{2.8}$$

where k_o is determined from a linear best fit to the calibration data. Thus

$$I(\rho) = (\rho/k_o)e^{-t/\tau}$$

or,

$$\rho = kI(\rho) \tag{2.9}$$

where

$$k = k_o e^{t/\tau} \tag{2.10}$$

where $I(\rho)$ is the count rate observed during flight at the time t (days) later than the calibration. The calibration data for the present flight

were obtained on 4/7/76, and are shown in Fig. 2.5. Water vapor and total pressure measurements were combined (Ref. 1.4) to yield the density with about 5% accuracy. The count rates C and N were read with scalers. The observed GM output count rates C are labelled with X's, and the data I corrected by use of (2.5) for tube dead-time are labelled with dots. The best linear fit to the low density I data is shown; it is seen that near 2 kcps the C data do fall perceptibly below the I data and both fall below the linear fit. From this figure we obtain

$$k_o = 1.14 \times 10^{-5} (kg/m^3)/cps \qquad (2.11)$$

The departure from linearity at high density is due to multiple scattering and is as expected (Ref. 1.1). For present purposes we limit the analysis to densities less than $2 \times 10^{-2} kg/m^3$, which is equivalent to about 30 km, so that the linear fit is applicable.

At low density in a vacuum chamber the "wall-effect" can cause the count rate to be larger than would be experienced in space. Since the scattering cross section is strongly Z dependent, however, it is possible to test for wall-effect as follows. The steel vacuum chamber is lined with a low-Z material, such as plastic, and the calibration curve is compared with that without the liner. With the low-Z liner the calibration curve will fall below that without it, if this effect is significant. Over the pressure range shown here no wall-effect was evident.

It is the count rate N that is determined from the telemetered and recorded pulses. N and C are related by

$$N = C/(1 + \tau_c C) \qquad (2.12)$$

From this equation we find

$$C/N - 1 = \tau_c C \qquad (2.13)$$

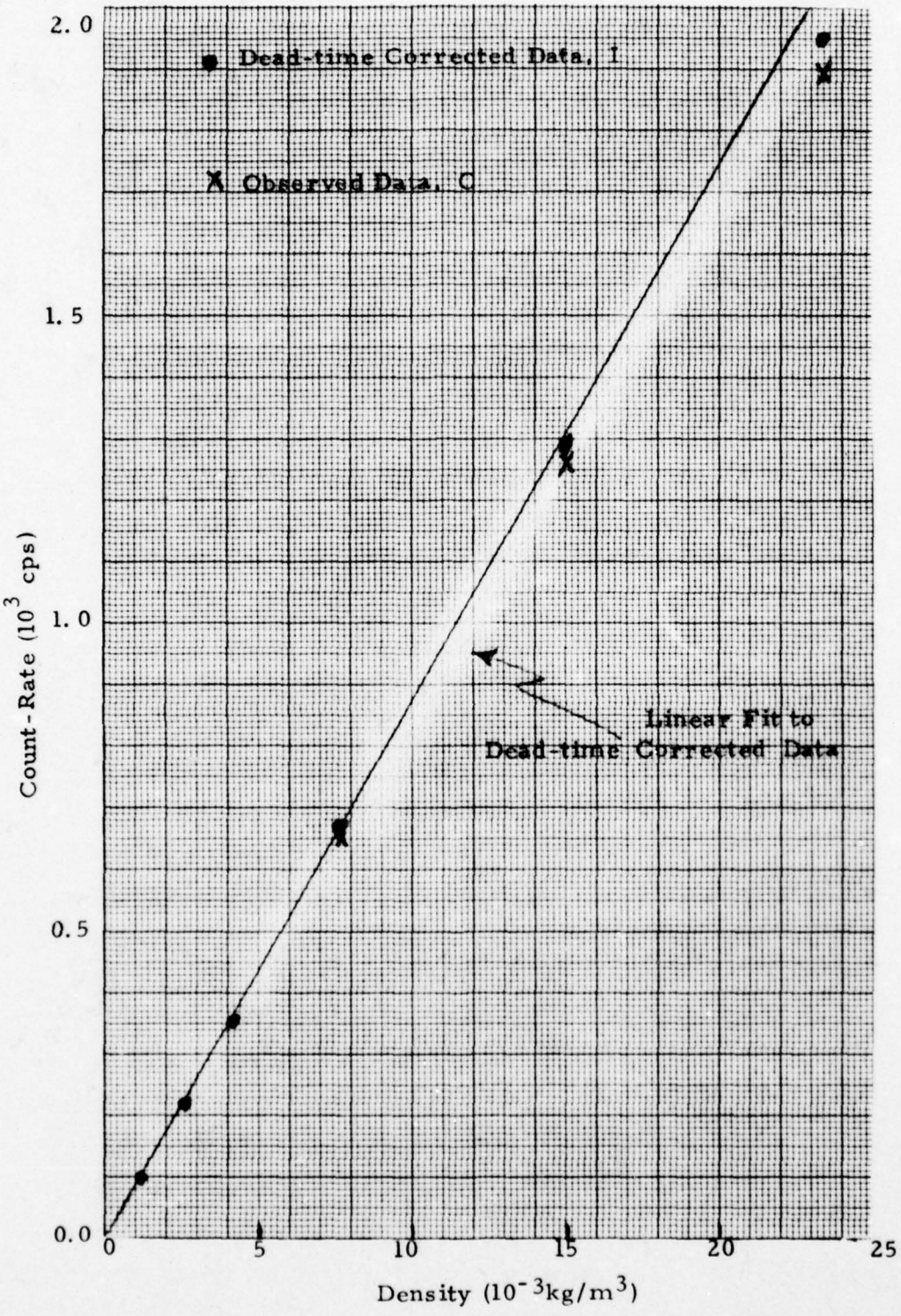

Fig. 2.5 Density Calibration Data For Low Background Betasonde, 4/7/76.

Thus, a test of the validity of (2.12) is provided by plotting C/N-1 vs C. This should be a straight line and the slope should agree with the design value for dead-time τ_c. Fig. 2.6 shows such a plot. The fit is linear and the shape leads to

$$\tau_c = 172\,\mu\text{sec} \tag{2.14}$$

which is as expected. Now we note that use of (2.13) in (2.5) for C leads to

$$I = N/(1 - \tau_e N) \tag{2.15}$$

where τ_e is the effective time constant of the entire system including GM tubes and dead-time circuit:

$$\tau_e = \tau_c + T_c \tag{2.16}$$

From (2.6) and (2.14)

$$\tau_e = 184.5\,\mu\text{sec} \tag{2.17}$$

An additional factor that must be taken into account is the cosmic ray background. By use of a six-hour integration this count rate was determined at Panametrics, Inc. in Waltham, MA to be ($h \approx 0$ km)

$$I_c = 0.023 \text{ cps} \tag{2.18}$$

for both tubes running sumultaneously. This count rate varies in a relatively well-defined manner with altitude (Ref. 1.1), having a peak 29 times the sea-level result near 20 km, decreasing monotonically to a value about 13 times sea-level at 50 km and remaining constant at that value for higher altitudes. The effect is most important at high altitude where the density-dependent count rate is low. The high altitude value for I_c is about .3 cps, which is only about 2% of the density dependent count rate at 65 km for the density calibration data of Fig. 2.5. Consequently, for present purposes it is sufficiently accurate to estimate

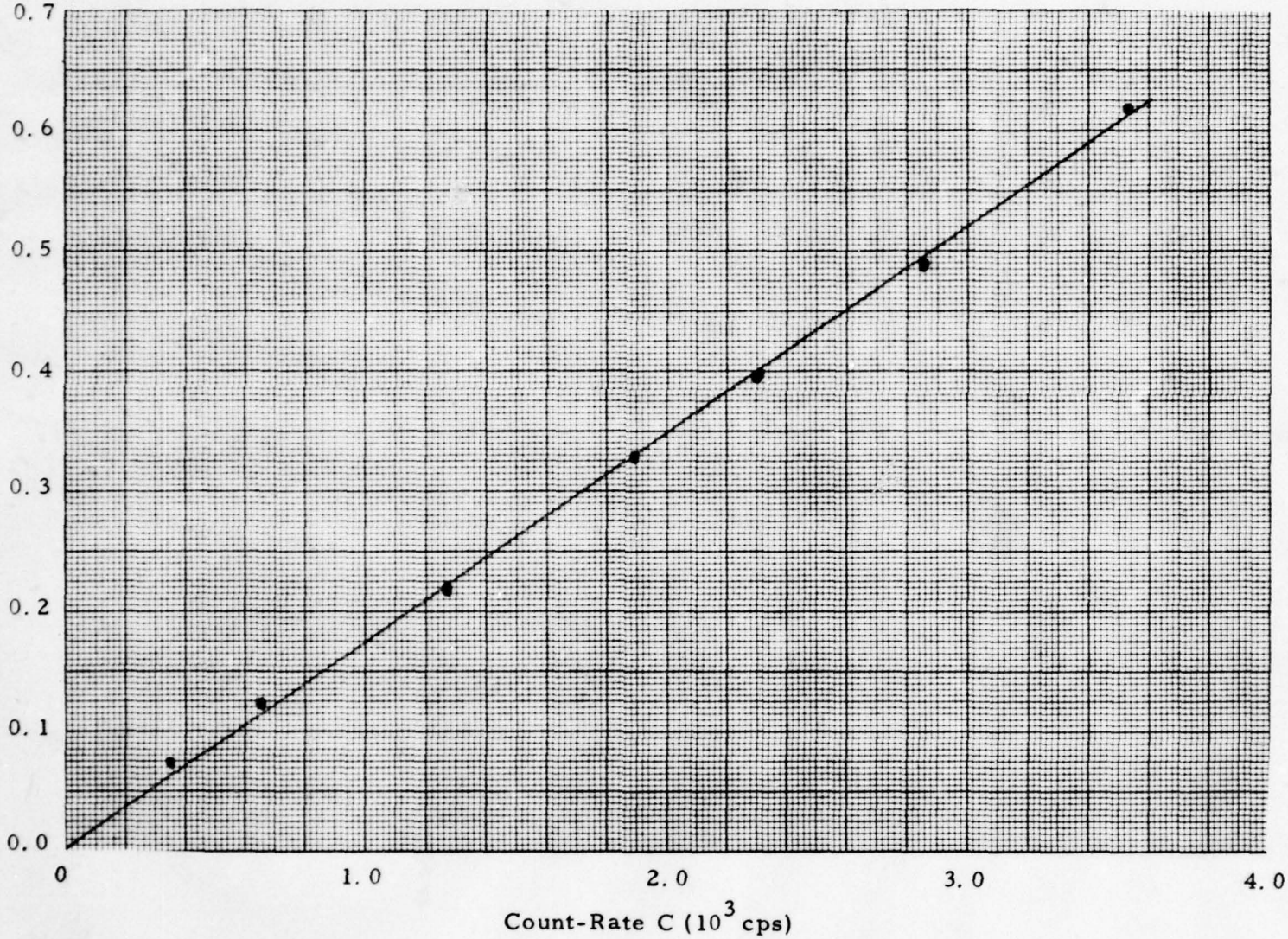

Fig. 2.6 Dead-Time Circuit Calibration Data.

this contribution to the count rate I by assuming the value of I_c to be 29(. 023) = . 67 cps at 20 km reducing linearly to the plateau value of 0. 3 cps at 50 km and remaining at that value above that altitude.

Thus, the procedure for finding $\rho(h)$ at altitude h from the calibration and flight data is as follows:

(1) The TM pulses are integrated over known time intervals (~1-5 seconds) and tabulated with the implied total count rate $N_t(h)$ and the radar-determined altitude h at the center of the time interval.

(2) The total count rate $I_t(h)$ is determined by use of $N_t(h)$ from (2. 15) and (2. 17).

(3) The density dependent count rate I(h) is determined from $I(h) = I_t(h) - I_c(h)$, where $I_c(h)$ is the cosmic-ray count rate at altitude h, as described above.

(4) In the general case the density ρ is determined from a curve (or analytic fit) of $I(\rho)$, Eq. (2. 7). In the high altitude region the density can be determined from (2. 9).

Once the values of N_t have been determined the statistical uncertainty in ρ can be found also. From Ref. 2. 2 the fractional uncertainty in I_t is

$$\frac{\Delta I_t}{I_t} = \frac{1}{\sqrt{N_t t_m}} \tag{2.18}$$

where t_m is the length of the measurement (1-5 seconds) at each altitude increment. For the linear relationship (2. 9), and where the cosmic ray count rate is low, this yields

$$\frac{\Delta \rho}{\rho} = \frac{1}{\sqrt{N_t t_m}} \tag{2.19}$$

Thus the fractional uncertainty is largest at high altitudes, where N_t is lowest.

2.4 Flight Results

2.4.1 Operational Analysis

The modified Betasonde was launched from White Sands Missile Range (WSMR) at 17:00:00 UT on April 23, 1976 on board an Arcas rocket. Just prior to apogee (approximately 65 km) the nose cone was ejected. After separation the sonde continued to climb to apogee, deployed the parachute, and began its descent. Good air density related count rate data were obtained from 4 sec. after separation at approximately 65 km down to an altitude of about 24 km. These results are discussed and plotted in the next section. A telemetry dropout occurred over the approximate altitude range of 24 km to 20 km. Valid data was obtained after this dropout down to approximately 1.5 km.

During the entire flight the temperature of the GM tubes was monitored with a thermistor and associated circuitry. This monitor shows that the GM tube temperature steadily increases from $+25^{\circ}C$ at 65 km to $+30^{\circ}C$ at 30 km. After reaching this maximum the temperature slowly decreases to $+25.5^{\circ}C$ at 25 km. Below this altitude the temperature steadily drops to a minimum of $-15^{\circ}C$ at 1.5 km at which altitude the TM signal becomes very noisy and LOS occurs. The flight duration from separation to LOS is approximately 27 minutes.

The telemetry link consisted of a pulse modulated 1680 MHz transmitter, as part of the sonde, and 2 independently operating GMD meteorological receivers for redundancy. This redundancy was a valuable feature during the flight since only one receiver worked well from launch to 17:16:00 UT and the other from that time on until LOS occurred. The received pulses, corresponding to the observed beta particle count rate multiplexed with the temperature monitor frequency, were recorded on magnetic tape. A counter and printer were in addition recording the data in real time. Both records are continuously correlated with time in one second intervals. The altitude versus time information was obtained from a radar tracking station.

In summary, the flight was successful and good data were obtained from about 65 km to 24 km and again from 20 km to 1.5 km. During the upper portion of the descent the temperature of the GM tubes remained fairly constant (+25°C to +30°C) and therefore the temperature effect on the count rate is negligible.

2.4.2 Density Results

The telemetered pulses were accumulated into $t_m = 5$ second intervals, and the procedure described in Section 2.3 was followed. The flight took place 16 days after the calibration, which leads to

$$k = 1.152 \times 10^{-5} (kg/m^3)/cps \qquad (2.20)$$

from (2.10) and (2.11). Results are shown in Figs. 2.7 and 2.8, along with the calculated statistical uncertainties from Eq. (2.19). Also shown for comparison is the mid-latitude Spring/Fall model atmosphere (Ref. 2.1). Agreement between the data and the model is extremely good; such agreement would certainly not occur in all cases. It is, nevertheless, very encouraging to obtain such agreement in at least one instance.

Useful count rate data were also obtained from about 20 km downward, in the very non-linear region of the density calibration curve. (See Ref. 1.1, for example.) A portion of the data are missing in the 20-25 km region as a result of TM dropout. It is our intent to reduce the available low altitude data also, and to develop a method of providing an analytical least-squares fit to the observed results for $\rho(h)$.

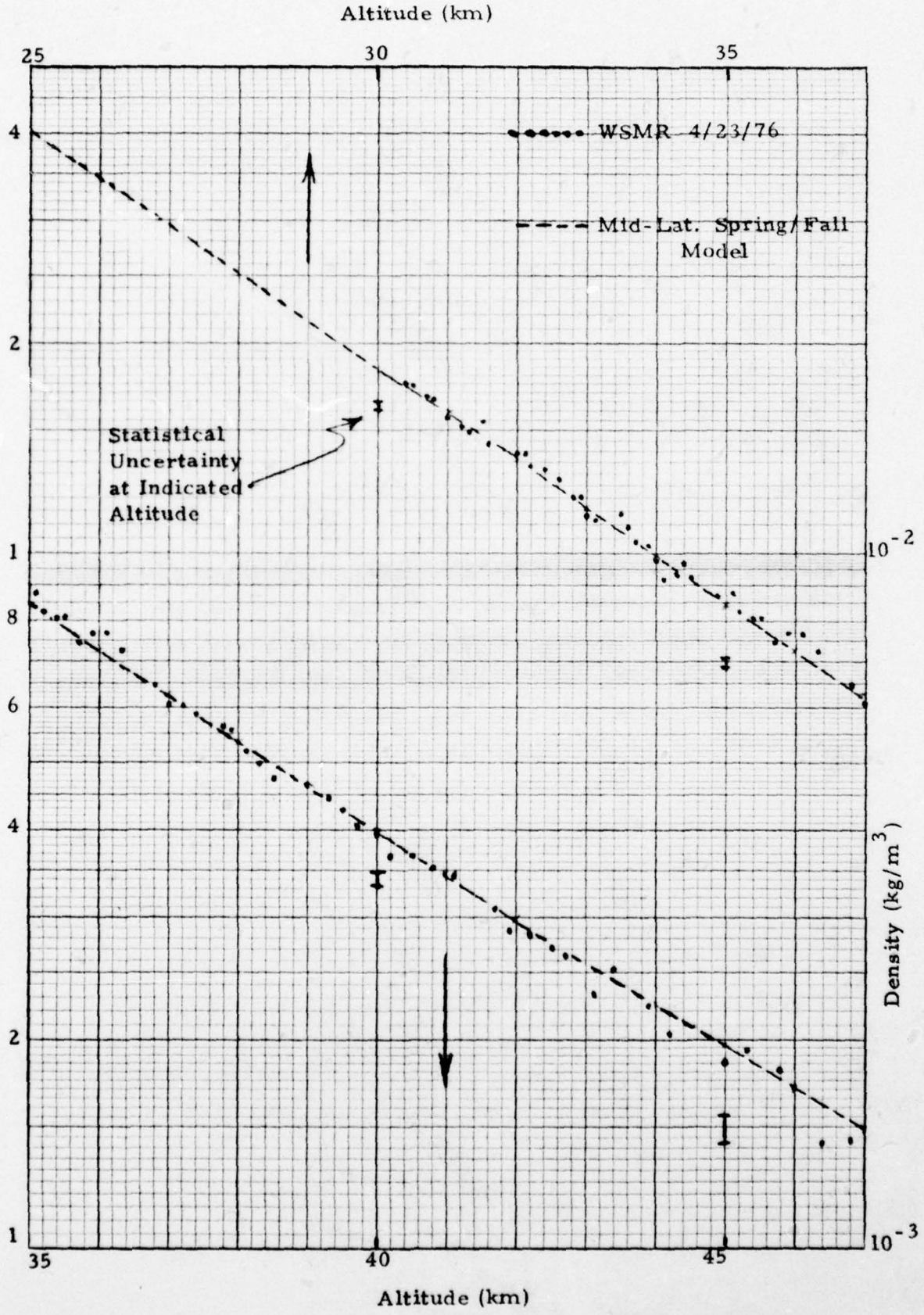

Fig. 2.7 Low Background Betasonde Air Density Results for Flight at White Sands Missile Range on 4/23/76, 30-45 km.

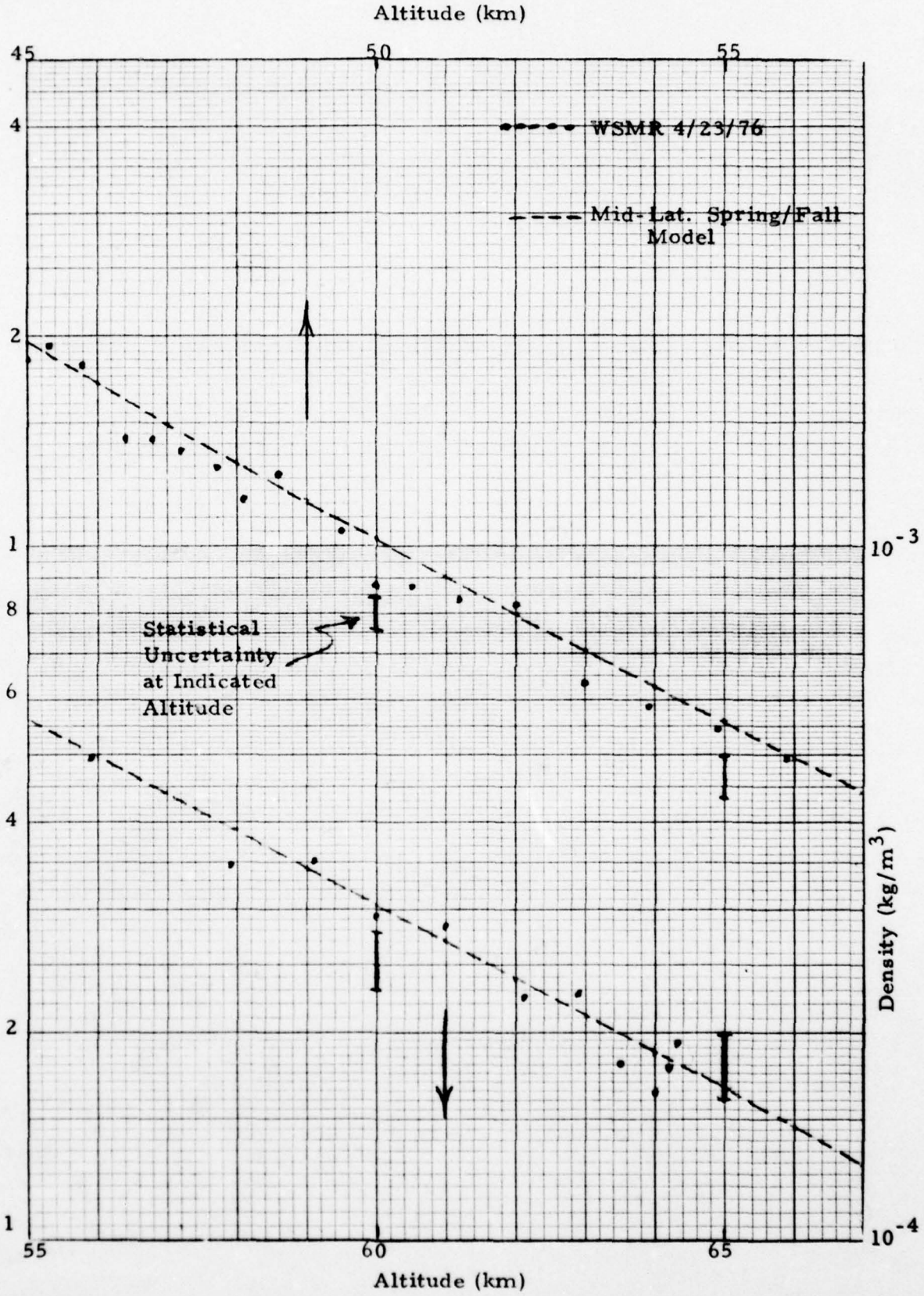

Fig. 2.8 Low Background Betasonde Air Density Results for Flight at White Sands Missile Range on 4/23/76, 45-65 km.

3. UV SPECTROPHOTOMETER

3.1 Modifications for Flight on Stratcom VI-A Balloon

A detailed description of the basic UV Spectrophotometer (UVS) is given in Ref. 1.7. To fly the UVS on a balloon for a prolonged period of time required several design changes to the basic instrument. They include increased thermal insulation, selection of the filter wheel sample rate by ground command, and the mounting configuration.

The basic instrument is equipped with an internal ON/OFF temperature control maintaining all components at a constant $+20^{\circ}C$. Power requirement for this control is 50W at 28V, when on. Due to power restrictions on this flight the heater control had to be disconnected, subjecting the instrument to the temperature extremes of the tropopause and mid-stratosphere. To maintain a reasonable thermal isolation between the ambient environment and the inside of the instrument the basic UVS was placed in an insulated cylindrical container. The overall dimensions of this cylinder are 15 in. by 12 in. diameter allowing for 3 in. of polyethylene insulation all around the instrument. Figure 3.1 shows an outline drawing of the instrument package. To minimize the effect of heat radiation at float altitude, the outside was painted with a high reflectivity/low emissivity vinyl epoxy paint. In order to maintain low outgassing properties of this package it was pressure sealed with O-rings.

The instrument package was mounted on a sun-seeking platform with its centerline at 45° from the vertical. Since the half angle of the optics of the UVS is 75°, light reflection from the balloon had to be obscured with an optically black shield.

The basic instrument has a fixed sample rate of the filter wheel of one sample per second, completing one spectrum scan in a total of 12 sec. Although this is desirable during ascent and descent of the payload, it is unnecessarily fast during long periods at relatively constant

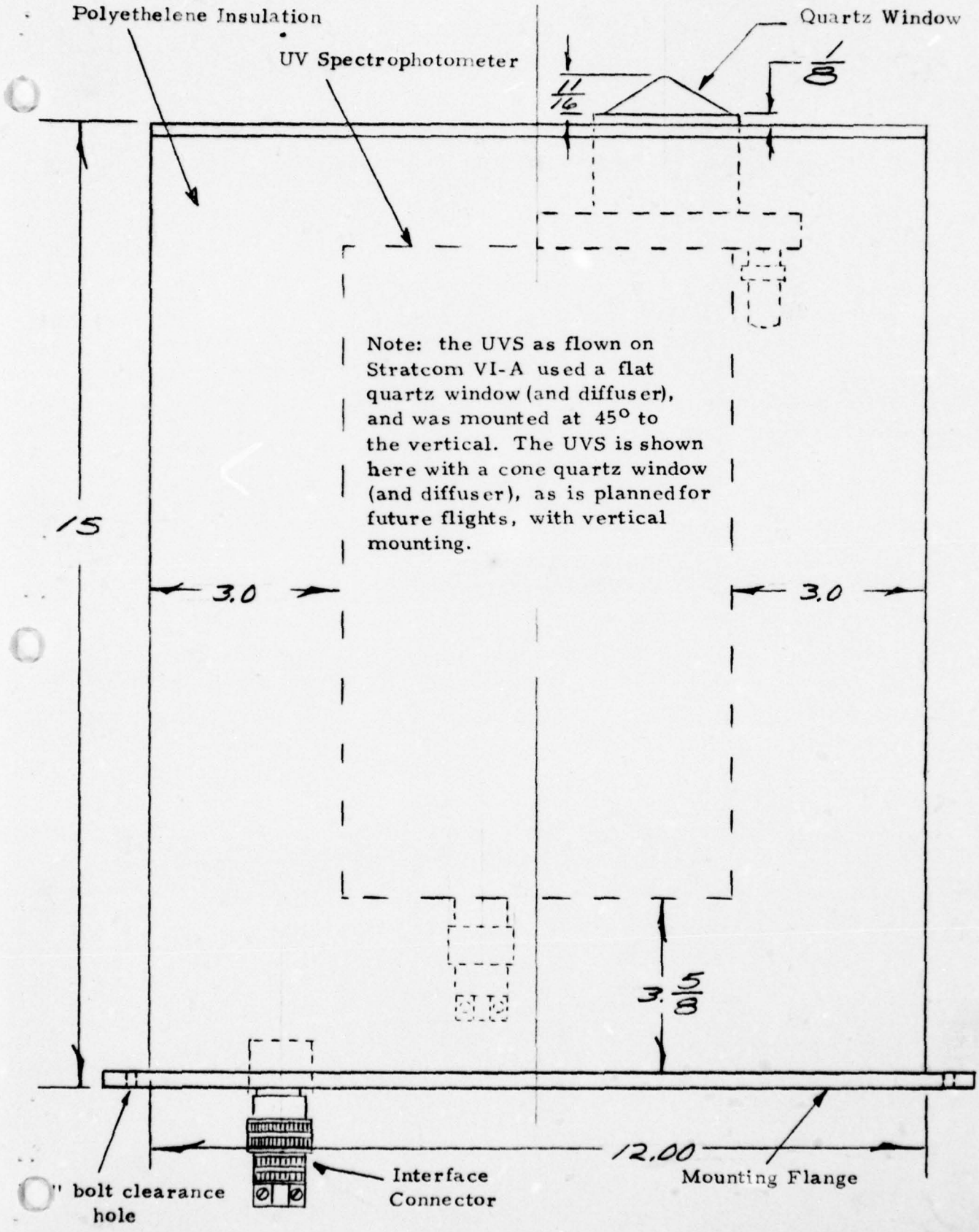

Figure 3.1 Outline Drawing of UVS Mounted Inside Thermally Insulating Container.

altitude. Therefore the design was modified to include a sample rate of one sample every 10 seconds, completing one scan in 120 seconds. Selection of the appropriate sample rate is effected by a simple contact closure, external to the instrument. On this balloon flight the sample rate was selected by ground command via the telemetry up-link.

3.2 Calibration

The calibration procedure has been described in Refs. 1.7 and 3.1. The response of the UVS to a calibrated Standard of Spectral Irradiance (SSI)* is measured and corrected for the difference in solar spectral shape. The result is a calibration constant in $A/(W/(cm^2\text{-}nm))$ for each filter set. The UVS was calibrated before and after the balloon flight with the internal temperature monitor at 25° to $30^{\circ}C$. Most filter sets showed only a few percent variation between the two calibrations. The average calibration is listed in Table 3.1, and this was used for the data reduction. Also listed are the single filter bandwidths and the number of filters used in each set. The 393 and 363 nm filters are both used with neutral density 4 filter.

During the balloon flight the UVS cooled significantly during the nights, and operated with internal temperatures as low as $-40^{\circ}C$. The UVS operated properly under these conditions, but the calibration validity was suspect at the lowest temperatures. Consequently the UVS was calibrated after the flight at several temperatures between $-40^{\circ}C$ and $+30^{\circ}C$. Small corrections to the 25 to $30^{\circ}C$ calibrations are required at the lower temperatures, and these were made during data analysis.

The SSI is calibrated over the range 250 nm to 2500 nm. For calibration of the 220 nm (3 x 214.0 nm filters) set the SSI spectrum below 250 nm was calculated from a $3100^{\circ}K$ blackbody spectrum normalized to the 250 nm calibration intensity. This extrapolated spectrum

*A 200W tungsten-iodine quartz envelope lamp calibrated by EG&G Inc., Electro Optics Division, Salem, Mass. The calibration is traceable to the National Bureau of Standards.

Table 3.1

UVS Calibration Sensitivities
for the Stratcom VI-A Balloon Flight

Filter set wavelength (nm)	Single filter bandwidth (nm)	Number of filters used	Solar Calibration Sensitivity (A/(W/(cm^2-nm)))
393.0	26.4	1	3.324×10^{-3}
363.0	28.0	1	1.947×10^{-3}
329.2	2.2	2	9.802×10^{-3}
319.3	2.0	2	2.337×10^{-2}
310.3	1.8	2	2.485×10^{-2}
305.3	2.0	2	3.871×10^{-2}
297.8	3.0	2	7.535×10^{-2}
290.7	2.4	2	1.673×10^{-1}
287.3	1.8	2	2.984×10^{-2}
220.*	28.0	3	3.508

*At high altitudes the average wavelength detected by the set of three 214.0 nm filters is 220 nm.

yields a calibration for the 220 nm filter set which is accurate to about 50%. To improve the 220 nm calibration accuracy the SSI relative spectrum was measured using the calibrated UV photomultiplier from the UVS and several broadband filters. This effectively transfers the UV photomultiplier calibration, which extends below 200 nm, to the SSI. Using this method the SSI intensity at 220 nm was found to be within 10% of the extrapolated blackbody spectrum. The 220 nm calibration is thus improved to about 20% absolute error. The error in the other filter calibrations are less than 10%.

3.3 Flight Results

3.3.1 Operational Analysis

The scientific payload with the UVS on board was launched on September 24 from Holloman AFB near midnight, MDT, or 0600 UT. The balloon reached its float altitude (126-128 kft) at 0315 MDT and remained at that altitude for 10 hours, then slowly descended to approximately 100 kft at 1900 MDT. During this period UV data were obtained from sunrise to sunset with a filter sampling rate of 1/sec for most of the day. The instrument was turned on continuously at sunrise and sunset but was on an intermittent schedule of 3 min. ON every 30 min. during the day. Because of thermal problems with the drive mechanism for the sun-seeking platform the UVS was not pointed at the sun at all times and therefore valid data were only obtained sporadically during the sunrise hours. A detailed evaluation of this data is given in the next section.

During the night the payload reached a minimum of ~90 kft and the UVS was turned on periodically in an attempt to keep the inside temperature at reasonable levels. The computer model study made at Sandia Laboratories of the internal temperature conditions versus time indicated a minimum temperature of -5°C. According to our on board monitor, with a range of +50 to -5°C, this objective was not achieved,

since the monitor saturated at -5°C sometime after reaching ~90 kft that night. The low interval temperature is no problem during the night, since the UVS is not operational during this period anyway. However, the low temperature did require gain corrections on the next day, September 25, and all through the final parachute descent.

Fortunately for this experiment, the multiplexed monitor output exhibits a temperature coefficient of its cycle time, which in no way influences the data, but which could later be used during a post calibration. This calibration was performed by placing the instrument in a cold chamber and applying a calibrated light source to stimulate the UV detector. In this way a correlation was obtained between cycle time and detector response at various chamber temperatures. Thus, a correction factor for the detector response versus cycle time resulted, which was then applied to the flight data. The largest correction factor encountered is -2.5% and occurs at sunrise on September 25. At approximately 10:00 MDT of the same day the payload was cut down and began its parachute descent. From sunrise to just before cut-down the filter sample rate was 0.1/sec and the instrument was turned on periodically. Prior to cut-down a ground command was sent which turned the instrument continuously ON and selected a filter sample rate of 1/sec. The flight was terminated at ~0439 MDT. As during the previous day the sun-seeking platform was inoperative for periods of time restricting the data gathering capability of the UVS. This problem with the platform is more serious during descent where data gaps occur over large altitude ranges due to the relatively fast descent rate. The flight data is discussed and tabulated in the next sections.

To summarize, good UV data were obtained on the balloon flight of September 24 and 25 at altitudes of up to 130 kft and during the parachute descent. Due to thermal problems with the sun-seeking platform, data gaps occurred during float as well as during the portion of parachute descent that occurred immediately after balloon cut-down.

3.3.2 Data Reduction Procedure

The basic data reduction procedure for the UVS has been described in Refs. 1.7, 3.1, and 3.2. For altitudes above about 20 km the effects of Rayleigh scattering become quite small, and so the analysis procedure is simplified. However, the large temperature variations experienced by the UVS on the Stratcom VI-A flight require additional corrections to the data because of voltage level and calibration shifts.

The UVS data for a complete cycle consists of 10 UV filter measurements for the wavelengths listed in Table 3.1, a dark current measurement, and two calibration points from the set (1, 2), (3,4), (5, CALB), and (CALA, 0). The values 0, ---, 5 are nominal voltage calibrations to correct for any shifts that might be introduced in signal transmission and processing, while CALA and CALB are light calibration points to monitor the photomultiplier-log amplifier gain.

The UV data are obtained from a strip chart recording or printout of the digitized data, and are normalized to the 0, ---, 5 volt levels taken as equal to their nominal values. The data are corrected to 20°C values by

$$V_{corr} = V_{nom} \times f_{corr}(T) - \Delta V_{corr}(T) \qquad (3.1)$$

where $f_{corr}(T)$ varies from 0.99 at 30°C to 0.975 at about -40°C, and $\Delta V_{corr}(T)$ is 0.00 at 20°C with -40°C values as given below:

item	ΔV_{corr}(-40°C)
CALA, CALB	+0.110
393, 363 nm	+0.057
other λ's	+0.017

The values for $f_{corr}(T)$ and $\Delta V_{corr}(T)$ are obtained from the post-flights calibration data which were taken at several instrument temperatures.

The measured fluxes are given by

$$F_m(\lambda) = (i_m(\lambda) - i_d)/(S_p(\lambda)R(\theta_{sd}, \lambda)\cos\theta_{sd}) - B_e(\lambda) \qquad (3.2)$$

with

$$i_m(\lambda) = 10^{V_{corr}(\lambda) - 10} \qquad (3.3)$$

i_d is (3.3) with the dark current voltage, $S_p(\lambda)$ is the calibration constant from Table 3.1, $R(\theta_{sd})$ is the diffuser relative angular response, and θ_{sd} is the sun line-diffuser normal angle. The leakage flux correction is

$$B_e(\lambda) = B_b(\lambda)F_m(363\text{ nm})R(\theta_{sd}, \lambda)/R(\theta_{sd}, 363) \qquad (3.4)$$

where $B_b(\lambda)$ is calculated from the measured filter transmission curves (see Ref. 1.7 for additional details). $B_b(393)$ and $B_b(363)$ are 0.0. Values for θ_{sd} were calculated from the balloon location, as obtained from tracking radar data, and sun location data from Ref. 3.3.

A final correction is made by

$$F_{corr}(\lambda) = F_m(\lambda) \times 10^{-\Delta V_{cal}} \qquad (3.5)$$

where

$$\Delta V_{cal} = \bar{V}_{corr}(CAL) - \bar{V}_o(CAL) \qquad (3.6)$$

with $\bar{V}_{corr}(CAL)$ the average of CALA and CALB from (3.1), and $\bar{V}_o(CAL)$ the average from the calibration data. The correction (3.5)

accounts for shifts in PM and log-amplifier gains. The results (3.5) are accurate to about 10% when the leakage flux $B_e(\lambda)$ in (3.2) is less than 25% of $F_m(\lambda)$.

The 220 nm measurements at high solar zenith angles required an additional correction, with

$$F_{corr}(220) = F_m(220) \times F_{tm} \tag{3.7}$$

where

$$F_{tm} = \frac{2}{\frac{F_{corr}(393)}{F_o(393)} + \frac{F_{corr}(363)}{F_o(363)}} \tag{3.8}$$

The correction (3.7) normalizes the 220 nm flux to the average 363-393 nm fluxes, since $F_o(\lambda)$ is the unattenuated solar flux at λ at 1 AU. Since the earth-sun distance during the Stratcom VI-A flight was 1.003 AU, all solar fluxes are essentially those at 1 AU, except as attenuated by ozone and oxygen. The final, corrected value for the flux at 220 nm is accurate to 20% when $B_e(\lambda)$ in (3.2) is not a large correction (< 25%).

For some wavelengths the residual ozone above the balloon can be calculated from

$$t_{O_3}(\lambda) = \frac{-\cos\theta}{\mu_{O_3}(\lambda)} \ln\left\{\frac{F_{corr}(\lambda)}{F_o(\lambda)} F_{tm}\right\} \tag{3.9}$$

The result (3.9) is most accurate for values of the bracket between about 0.3 and 0.05.

3.3.3 Data

Stratcom VI-A was launched during the night of Sept. 23-24, 1975, and was at float altitude of 127 kft by 0400 MDT (=1000 GMT). Radar contact was lost between 0545 MDT and 1100 MDT (1145 to 1700 GMT), during the first sunrise. The balloon was at 127 kft near 34°N latitude, 107°W longitude, from about 0400 MDT to 0545 MDT, and at 128 kft near 34°N latitude, 107°W longitude, from 1100 MDT to 1130 MDT, when the slow descent began. It thus seems quite likely that during the first sunrise the balloon was at 127.5 kft near 34°N, 107°W, and the UVS data have been analyzed using this balloon location. For all other times the radar tracking data have been used for the balloon location.

The UVS data can be conveniently separated into four groups: sunrise on Sept. 24; sunset on Sept. 24-25; sunrise on Sept. 25; and parachute descent after cut-down on Sept. 25. The sunset data span two days in GMT and hence are listed as Sept. 24-25. All times listed with the UV data are in GMT (hours-minutes). Although the UVS was mounted on a rotating platform with a sun sensor, it generally took more than an hour after sunrise for the mechanism to warm up sufficiently for proper operation, and so the sunrise UV data are limited to chance payload rotations which pointed the UVSat the sun.

The UVS solar flux data for the four periods listed above are given in Tables 3.2 to 3.5. Fluxes were calculated as described in the preceeding section. All 220 nm fluxes have been normalized to the 393 and 363 nm measurements, except where no corresponding measurements are available. The fluxes are for an area perpendicular to the sun-earth line, and do not include any backscattered light from the lower atmosphere and the earth's surface. The sun-earth distance for Sept. 24-25 is 1.003 AU, so solar UV fluxes not attenuated by ozone or oxygen are effectively normalized to 1 AU. The uncertainty in the fluxes is $\pm$10%,

Table 3.2
Stratcom VI-A
UVS Solar Flux Data for Sunrise on Sept. 24, 1975

GMT (hrs-min)	Altitude (kft)	Sun zenith angle (deg)	Flux (W/(cm^2-nm)) at wavelength λ (nm), on an area normal to the sun-earth line*									
			393	363	329.2	319.3	310.3	305.3	297.8	290.7	287.3	220
1244	127.5	93.6	6.42-5	4.25-5	7.23-6	1.06-6	1.68-8	(1.20-8)	-	-	-	-
1249	127.5	92.5	1.07-4	9.03-5	4.57-5	(5.06-6)	(7.59-8)	(8.60-8)	-	-	-	-
1352	127.5	79.6	-	-	-	-	-	-	-	-	-	8.92-8
1509	127.5	64.1	1.18-4	1.11-4	1.18-4	7.47-5	6.26-5	5.38-5	3.56-5	2.12-5	(1.15-5)	8.77-7
1521	127.5	61.7	1.18-4	1.14-4	1.19-4	7.88-5	6.13-5	5.65-5	3.65-5	2.40-5	(1.26-5)	1.05-6
1642	127.5	47.3	1.22-4	1.11-4	1.20-4	8.00-5	6.65-5	5.99-5	4.02-5	3.10-5	(1.46-5)	1.41-6
1705	128.0	43.5	1.19-4	1.13-4	1.20-4	7.96-5	6.48-5	6.11-5	4.10-5	3.16-5	(1.57-5)	1.44-6
1834	126.1	34.7	1.09-4	9.85-5	1.06-4	7.05-5	5.88-5	5.42-5	3.38-5	2.80-5	(1.29-5)	1.37-6

*6.42-5 ≡ 6.42×10^{-5}. Numbers in parentheses are for measurements where the leakage flux is greater than 25% of the solar flux measurement, and so have increased uncertainty. Blanks indicate either that no measurement was obtained because of payload rotation, or the flux is too low to measure reliably.

Table 3.3
Stratcom VI-A
UVS Solar Flux Data for Sunset on Sept. 24-25, 1975

GMT (hrs-min)	Altitude (kft)	Sun zenith angle (deg)	Flux ($W/(cm^2-nm)$) at wavelength λ (nm), on an area normal to the sun-earth line*									
			393	363	329.2	319.3	310.3	305.3	297.8	290.7	287.3	220
1933	124.8	35.1	1.16-4	1.00-4	1.10-4	6.96-5	6.20-5	5.47-5	3.41-5	2.71-5	(1.29-5)	1.23-6
2023	122.1	39.6	1.18-4	1.09-4	1.17-4	7.61-5	6.16-5	5.43-5	3.52-5	2.29-5	(1.14-5)	9.87-7
2137	116.7	50.8	1.35-4	1.22-4	1.34-4	8.40-5	6.80-5	5.74-5	3.51-5	1.39-5	(9.11-6)	5.20-7
2238	111.8	62.0	1.22-4	1.18-4	1.19-4	7.00-5	5.38-5	4.15-5	2.27-5	3.79-6	(6.43-6)	1.32-7
2334	106.6	73.1	1.37-4	1.23-4	1.23-4	7.43-5	4.64-5	2.78-5	(1.41-5)	(8.18-7)	-	1.36-8
2341	106.0	74.5	1.31-4	1.21-4	1.24-4	7.12-5	4.26-5	2.44-5	(1.31-5)	(6.88-7)	-	8.84-9
0003	104.1	78.9	1.44-4	1.26-4	1.26-4	6.90-5	3.38-5	1.76-5	(9.40-6)	(5.35-7)	-	(1.89-9)
0010	103.5	80.2	1.32-4	1.19-4	1.16-4	5.71-5	2.70-5	1.23-5	(7.00-6)	(4.53-7)	-	(9.79-10)
0022	102.5	82.6	1.32-4	1.22-4	1.17-4	5.72-5	2.11-5	7.83-6	(5.08-6)	(3.89-7)	-	(3.84-10)
0035	101.5	85.2	1.27-4	1.15-4	1.05-4	4.60-5	1.12-5	2.84-6	-	(2.49-7)	-	-
0046	100.9	87.4	1.26-4	1.14-4	9.67-5	3.12-5	3.96-6	7.86-7	-	-	-	-
0059	100.4	90.1	1.19-4	9.25-5	6.04-5	(8.34-6)	(1.91-7)	(1.38-7)	-	-	-	-
0110	99.6	92.2	5.54-5	3.63-5	8.59-6	(7.86-7)	-	(1.70-8)	-	-	-	-
0119	98.3	94.0	9.34-7	4.37-7	1.26-7	(1.02-8)	6.11-9	3.97-9	-	-	-	-

*See footnote for Table 3.2

Table 3.4
Stratvom VI-A
UVS Solar Flux Data for Sunrise on Sept. 25, 1975

GMT (hrs-min)	Altitude (kft)	Sun zenith angle (deg)	Flux (W/(cm^2-nm)) at wavelength λ (nm), on an area normal to the sun-earth line*									
			393	363	329.2	319.3	310.3	305.3	297.8	290.7	287.3	220
1251	118.4	95.1	1.17-7	8.58-8	4.50-8	(1.15-8)	1.49-9	4.14-10	-	-	-	-
1308	120.8	91.5	1.30-4	1.08-4	6.68-5	(1.19-5)	(2.54-7)	(1.40-7)	-	(8.83-9)	-	-
1318	122.1	89.6	1.38-4	1.23-4	1.03-4	3.76-5	-	-	-	-	-	-
1322	122.6	88.6	1.41-4	1.26-4	1.19-4	5.67-5	1.39-5	-	-	-	-	(8.54-10)
1327	123.1	87.6	-	-	-	-	-	-	-	-	-	(1.35-9)
1329	123.4	87.1	-	-	-	6.98-5	3.15-5	1.28-5	-	-	-	-
1333	123.7	86.3	1.39-4	1.15-4	-	-	-	-	-	-	-	-
1337	123.9	85.6	-	-	-	7.16-5	3.88-5	1.99-5	-	-	-	-
1339	124.0	85.1	-	-	-	-	3.84-5	2.25-5	(1.35-5)	-	-	-
1342	124.1	84.5	1.43-4	1.25-4	1.09-4	-	-	-	-	-	-	-
1344	124.3	83.9	1.03-4	-	-	-	-	-	-	-	-	1.91-8
1349	124.8	82.9	1.25-4	9.71-5	-	-	4.80-5	2.88-5	(1.55-5)	1.24-6	-	3.17-8
1558	130.2	57.1	1.18-4	1.10-4	1.22-4	7.71-5	6.59-5	5.79-5	3.97-5	3.01-5	(1.47-5)	1.41-6
1600	130.1	56.8	1.15-4	1.12-4	1.18-4	7.85-5	6.36-5	5.60-5	3.81-5	3.05-5	(1.44-5)	1.44-6

*See footnote for Table 3.2

Table 3.5
Stratcom VI-A
UVS Solar Flux Data for Parachute Descent on Sept. 25, 1975

GMT (hrs-min)	Altitude (kft)	Sun zenith angle (deg)	Flux (W/(cm^2-nm)) at wavelength λ(nm), on an area normal to the sun-earth line*									
			393	363	329.2	319.3	310.3	305.3	297.8	290.7	287.3	220
[1600	130.1	56.8	1.15-4	1.12-4	1.18-4	7.85-5	6.36-5	5.60-5	3.81-5	3.05-5	(1.44-5)	1.44-6]
(Cut-down)												
1602	106.2	56.4	-	-	1.18-4	6.91-5	4.74-5	3.90-5	2.58-5	3.26-6	-	-
1603	91.0	56.2	9.96-5	1.02-4	1.21-4	7.01-5	3.98-5	2.39-5	(1.39-5)	(6.89-7)	-	7.22-9
1604	83.3	56.0	1.18-4	1.05-4	9.73-5	5.93-5	2.99-5	1.40-5	(8.57-6)	(5.27-7)	-	(2.61-9)
1606	73.9	55.7	1.18-4	1.03-4	9.52-5	5.64-5	2.38-5	1.02-5	(7.77-6)	(4.03-7)	-	(1.63-10)
1607	68.6	55.5	1.05-4	1.02-4	8.38-5	4.34-5	2.11-5	7.69-6	(4.16-6)	(3.29-7)	-	-
1608	62.3	55.3	9.66-5	9.85-5	1.01-4	4.99-5	2.03-5	7.41-6	(6.12-6)	(3.53-7)	-	-
1610	55.9	55.0	8.97-5	9.75-5	1.00-4	4.93-5	1.79-5	6.52-6	(6.05-6)	(3.34-7)	-	-
(1613	45.2	54.3	9.26-5	8.99-5	8.18-5	2.90-5	1.67-5	5.56-6	(4.86-6)	(3.15-7)	-	-)

*See footnote for Table 3.2

except for the 220 nm flux which is $\pm$20%. Numbers in parentheses have larger uncertainties because of large corrections for leakage flux at longer wavelengths. Blanks in the tables indicate either fluxes too weak to measure with the UVS, or that payload rotation did not give a sun view for that particular filter set.

Plots of solar flux vs. solar zenith angle for some of the sunset data of 24-25 Sept., from Table 3.3, are given in Fig. 3.2. Since the balloon was descending from 125 to 98 kft, the increasing attenuation with solar zenith angle is greater than if the balloon were at a constant altitude. Comparison of the data in Tables 3.2 and 3.3 show greater attenuation for the lower altitude sunset data, when compared at about equal solar zenith angles (compare also with the data in Table 3.4). The 320 to 300 nm region also show a modified "umkehr" effect for solar zenith angles greater than 90°, where the ratio of solar fluxes (e.g. J(305.3)/J(393)) first decreases with increasing zenith angle, and then flattens and increases slightly beyond 90°.

Some of the parachute descent data of Table 3.5 are plotted in Fig. 3.3. Here the attenuation is due primarily to the increasing ozone above the UVS as it descends through the ozone layer. The data below about 60 kft have more than a 10% uncertainty, since Rayleigh scattering becomes increasingly important at low altitudes. The 305.3 nm data show that the ozone layer lies mostly between 70 and 110 kft.

The high altitude data can be used to obtain an absolute value for the solar flux at 220 nm. This is done by plotting the measured intensities against the attenuation path length on a semilog plot and extrapolating to zero path length. The attenuation pathlength should be proportional to the local atmospheric pressure divided by the cosine of the solar zenith angle, provided that the oxygen/ozone ratio remains constant. Appropriate portions of the 24 Sept. sunrise, and 24-25 Sept. sunset data are plotted in Fig. 3.4, along with the best fit lines for data

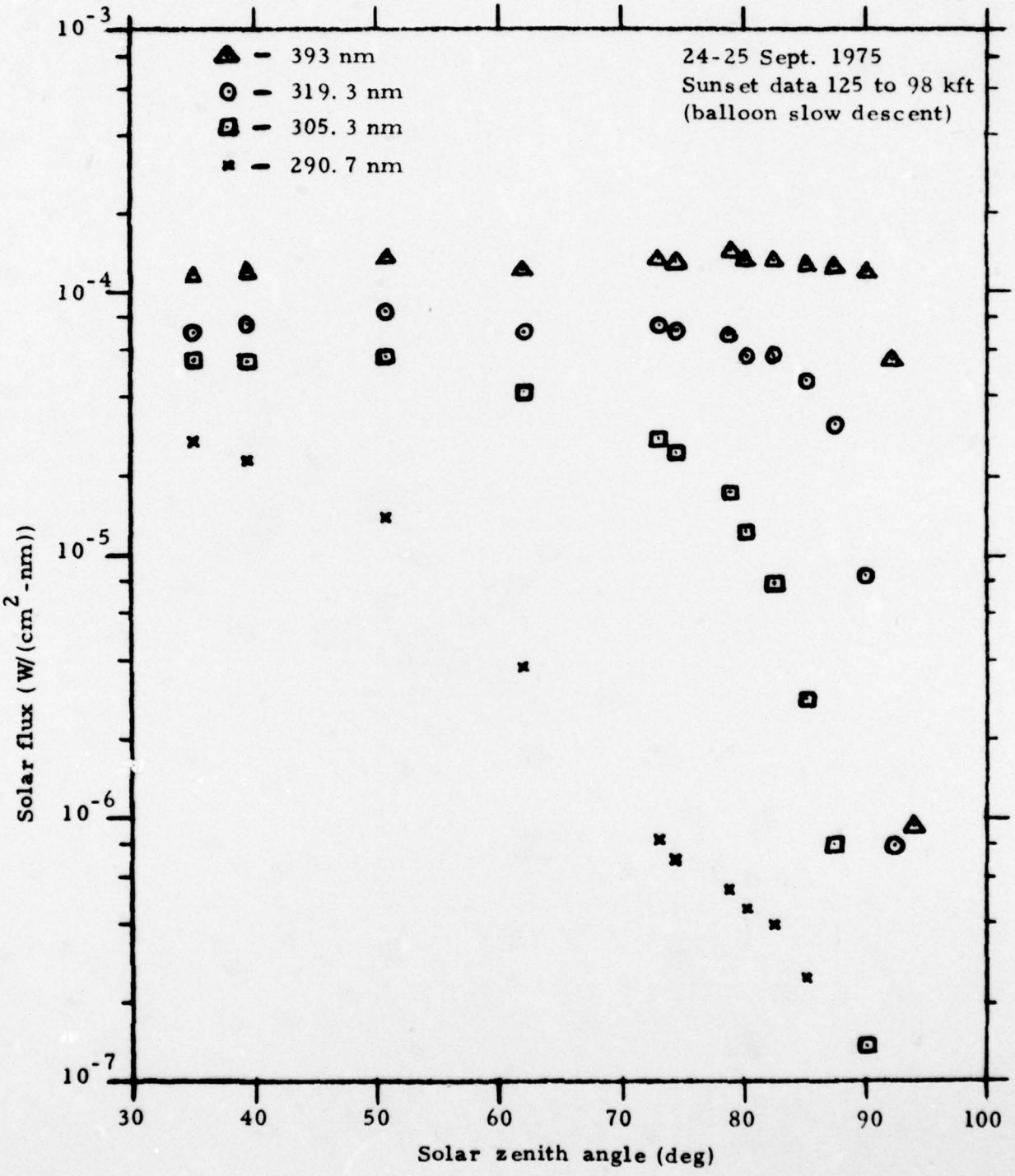

Fig. 3.2 Plot of Solar Flux vs. Solar Zenith Angle at Selected Wavelengths for Sunset on 24-25 Sept. 1975.

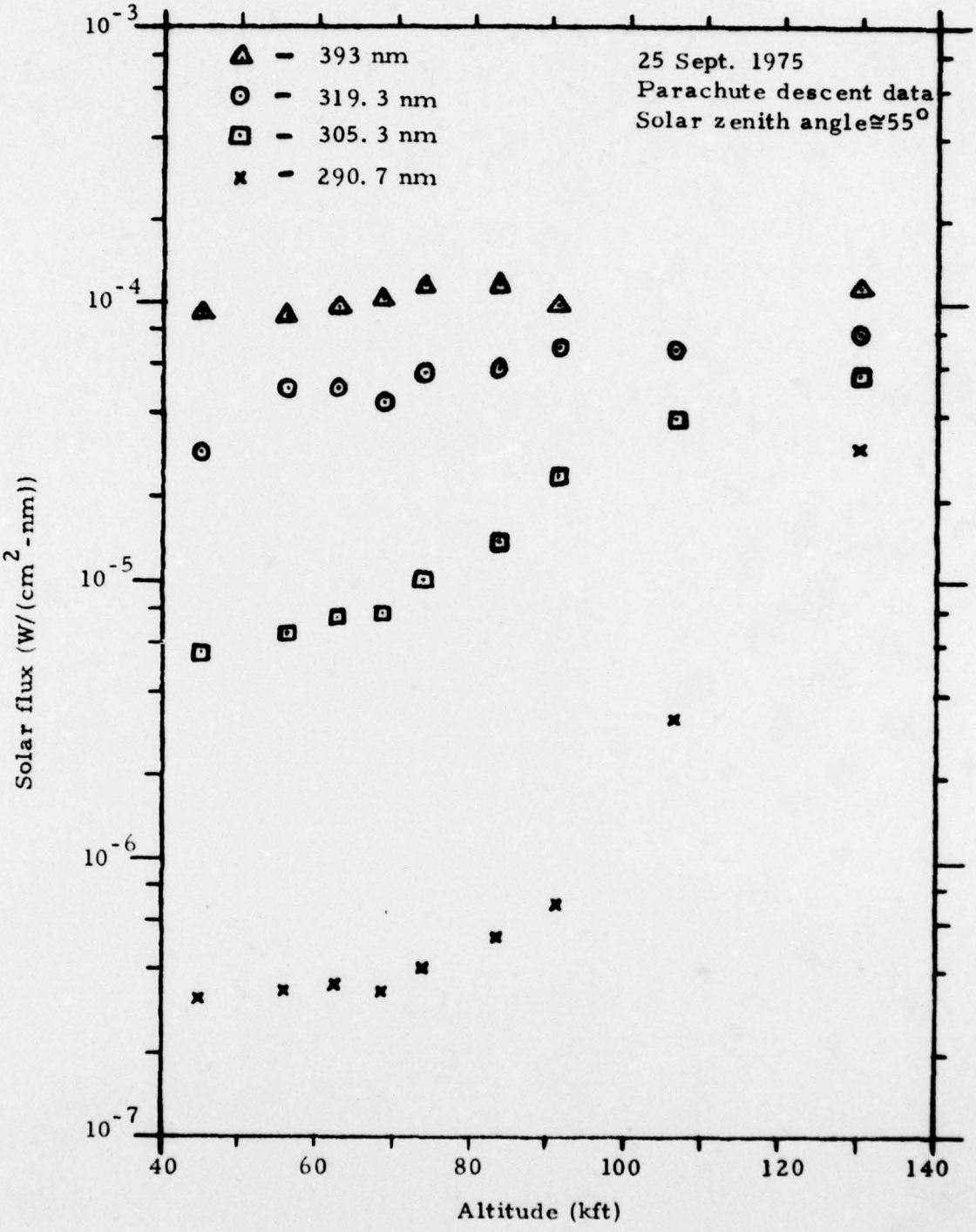

Fig. 3.3 Plot of Solar Flux vs. Altitude at Selected Wavelengths for Parachute Descent on 25 Sept. 1975.

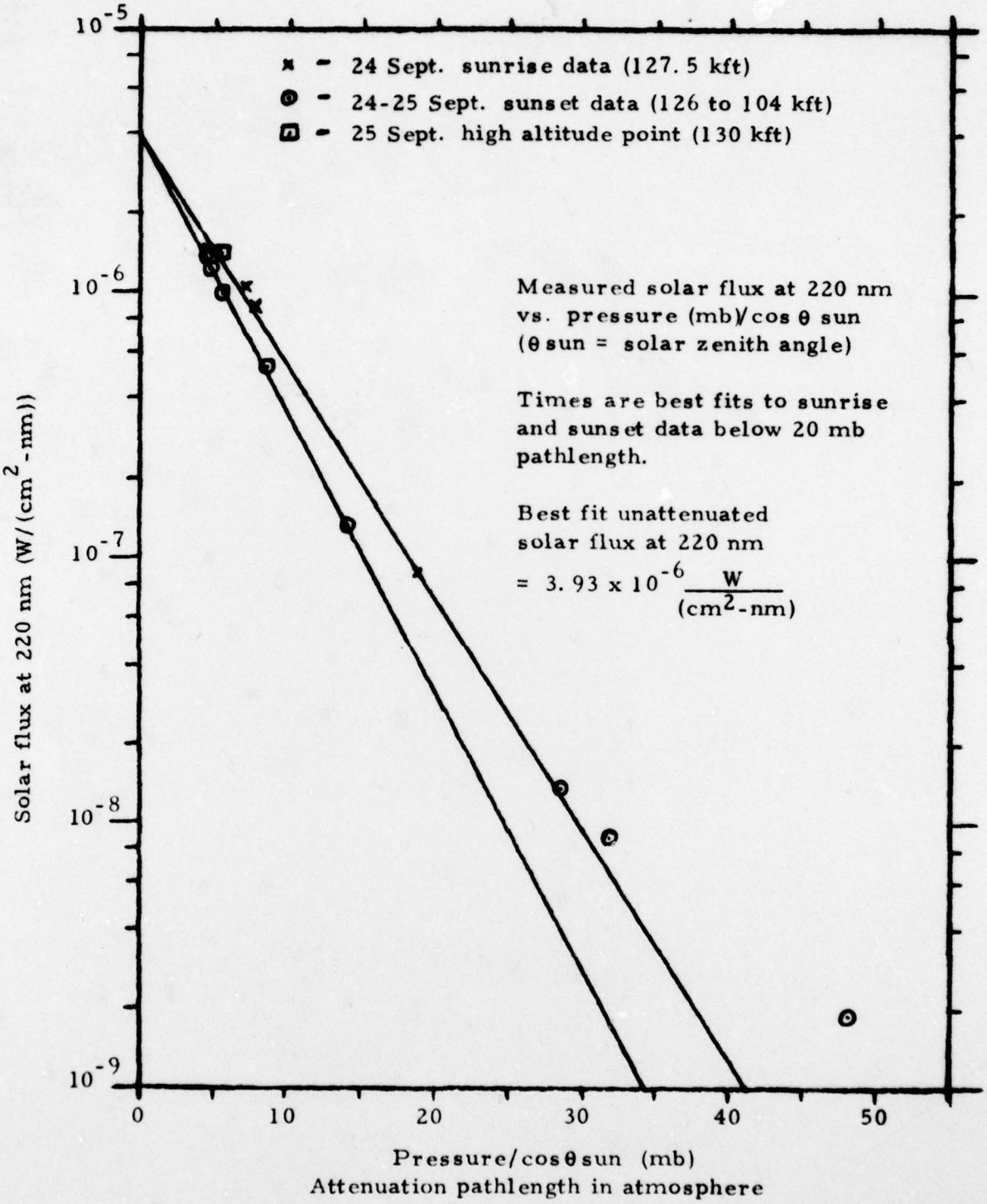

Fig. 3.4 Plot of Measured Solar Flux at 220 nm vs. Attenuation Pathlength in Atmosphere.

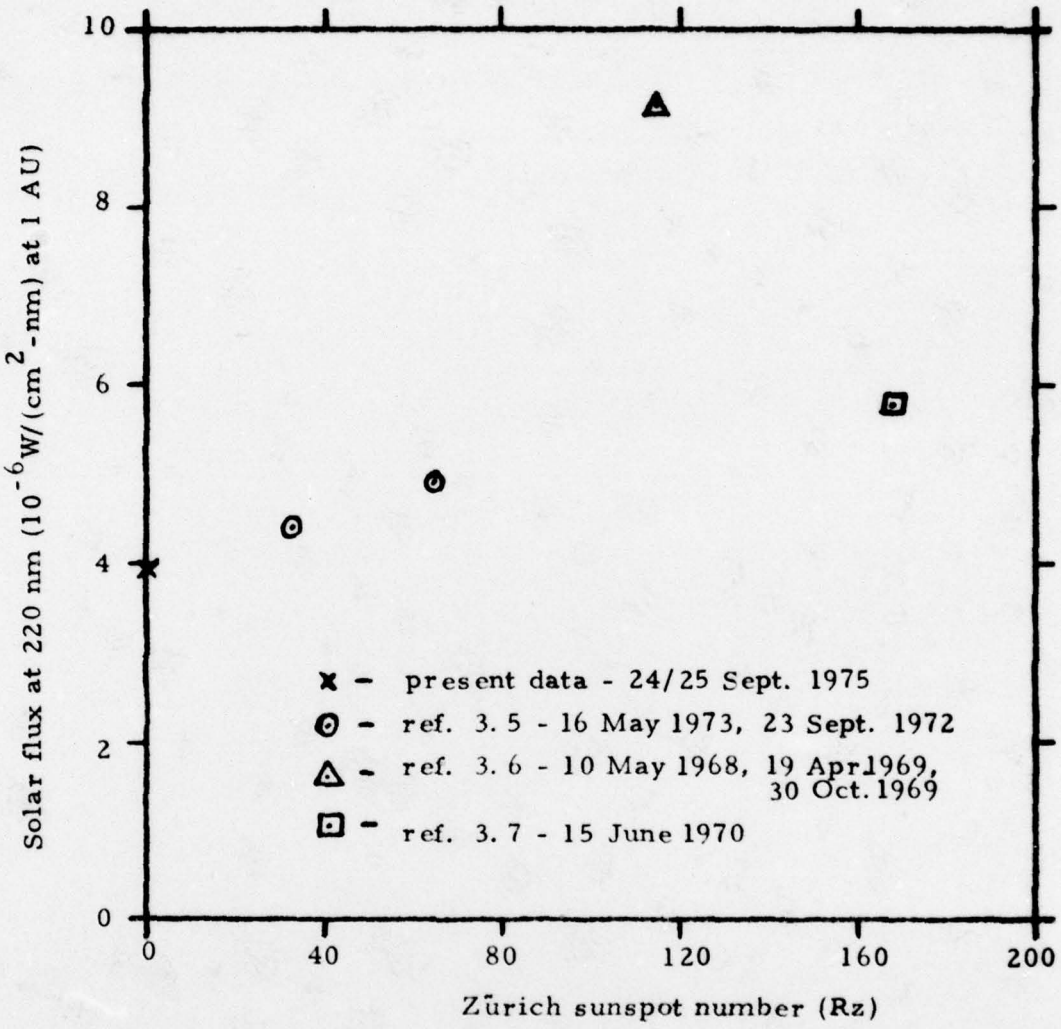

Fig. 3.5 Plot of Solar UV Flux at 220 nm vs. Sunspot Number

with $P/\cos\theta_{sun}$ less than 20 mb. The pressures were taken from the mid-latitude Spring-Fall model of Ref. 2.1. The 24 Sept. sunrise data have a nearly constant oxygen/ozone ratio, while the 24-25 Sept. sunset data has this ratio decreasing as the balloon descends. This accounts for the different slopes in Fig. 3.4. The zero pressure intercept is $3.93 \times 10^{-6} W/(cm^2 - nm)$, to 0.5% for both lines. The unattenuated solar flux at 220 nm (averaged over ± 5 nm, effectively), is thus measured to be $3.93 \times 10^{-6} W/(cm^2 - nm) \pm 20\%$ at 1 AU on 24-25 Sept. 1975.

The solar flux at 220 nm has been measured by a number of other groups over the past several years. Variations in the measurements are frequently larger than the quoted errors. The 220 nm flux given above is low compared to other recent measurements. Satellite data on solar UV show that variability increases as the wavelength decreases (Ref. 1.12). To check the variability of the solar 220 nm flux, the measurements of a number of groups have been compared with sunspot number, a measure of solar activity. In Ref. 3.4 the Zürich sunspot numbers Rz for 24-25 Sept. 1975 are given as 0. Solar flux measurements in Ref. 3.5 are an average for 16 May 1973 and 23 Sept. 1972, for which Rz is 33 and 65. Graphical results indicate that the flux at 220 nm was about 10% different on these two dates, so the average has been raised and lowered by 5% to give effective fluxes for those two dates. Ref. 3.6 gives an average flux measurement for data from 10 May 1968, 19 April 1969, and 3 Oct. 1969, for which Rz is 117, 128, and 99. The data in Ref. 3.6 are difficult to separate according to date, so the average flux at 220 nm has been used with the average Rz. Measurements in Ref. 3.7 are for 15 June 1970, when Rz was 168. The measured fluxes and sunspot numbers are listed in Table 3.6, and plotted in Fig. 3.5.

Table 3.6

Solar Flux at 220 nm vs. Zürich Sunspot Number

Solar Flux at 220 nm (±5 nm) ($W/(cm^2\text{-}nm)$)	Zürich Sunspot Number	Date of Measurement	Data source and comments
3.93×10^{-6}	0	24-25 Sept. 1975	Present results
4.39×10^{-6}	33	16 May 1973	Ref. 3.5 - average separated (see text)
4.91×10^{-6}	65	23 Sept. 1972	
9.16×10^{-6}	115	10 May 1968, 19 Apr 1969, 3 Oct. 1969	Ref. 3.6 - average Rz for 3 dates
5.78×10^{-6}	168	15 June 1970	Ref. 3.7

The data in Fig. 3.5 show a general rise in the 220 nm solar flux with increasing Rz. A possible peaking may exist near Rz = 100, but the data are too few to show this with certainty. The Rz values in Fig. 3.5 are the daily averages, but for the 220 nm region it may be better to use Rz averaged over a solar rotation. The data in Ref. 1.12 show that below 200 nm the solar UV flux varies significantly in a solar rotation, while at longer wavelengths the variations are more long-term. Thus the 27-day-averaged Rz may be a better index of solar UV variability for wavelengths greater than 200 nm.

Future measurements of the 220 nm flux, particularly during the coming several years as the sunspot cycle goes from minimum to maximum, will produce data of considerable interest by fixing more precisely the variability of the solar flux in this region. The variation of solar flux with altitude measured under this program will make it possible to check radiation transport model predictions. Finally, the calculation of UV flux at any altitude and point in the solar cycle can then be made with confidence and reasonably well known limits on the accuracy.

4. CONCLUSIONS AND RECOMMENDATIONS

4.1 Low-background Betasonde

The parachute descent of the Low-background Betasonde after release from the Arcas rocket yielded good air density data from 65 km to below 5 km. The Betasonde operated properly during the entire descent, with only a portion of the 20-24 km data being lost because of TM dropout. We believe that for the Betasonde, consideration should be given to eliminating the transmitter and recording the data on-board for later analysis. Solid-state data recording and readout techniques are now available that make such a development possible. In order to do this it would be necessary to count the pulses on-board in one second intervals, thus forming a 12-bit word each second, and recording ~2000 such words for a half-hour flight. The solid-state memory could then be removed and read shortly after the flight and, ultimately, a density profile could be printed out almost immediately. Such a development would completely eliminate the necessity for tracking the payload with TM receivers and would, therefore, also eliminate the possibility of data loss such as that which occurred on this flight. It should be noted that such a recorder could also be used with analog sensors, such as thermistors, by the addition of an analog-digital converter.

The data above 30 km have been reduced to air density and agree very well with the mid-latitude Spring/Fall model atmosphere. The data below 30 km require more elaborate analysis to yield air density, and will be reduced in the future. Methods for least-square fitting the air density data will also be developed.

The rather good agreement with the mid-latitude Spring/Fall model is partly fortuitous, since there are model variations with both latitude and season. The 45°N July model, e. g. , has a density at 60 km which is 20% greater than the mid-latitude (30°-60°) Spring/Fall model (Ref. 2. 1). Since the shift from the July to the Spring/Fall model is

gradual, there can at times be a substantial uncertainty as to which model, or interpolation between models, is most appropriate. This uncertainty is heightened by phase shift uncertainty in the seasons (an early spring or a late fall, e.g.), and amplitude uncertainty (a warm (cold) summer(winter), e.g.). Events such as sudden stratospheric warmings can produce more uncertainty as to the most appropriate density model to use. For events requiring a precise knowledge of the upper atmosphere density, it is thus best to make an in-situ measurement, such as with the Betasonde, at a time close to that when the density information is required.

Additional flights of the Low-background Betasonde are desirable to help define better the variability in the upper atmosphere density. Under sponsorship of the Army Research Office a model of the Betasonde, designated Betasonde II, is being developed by Panametrics, Inc. This sonde will use semiconductor detectors and improved radioactive sources, thus allowing its use to even higher altitudes without cosmic-ray background limitations. Fabrication of the improved sonde itself will not take place for about two years. However, the Low-background Betasonde has now been proven and will be available for use in the interim period to altitudes of at least 65-70 km. If possible, several flights during periods of rapidly changing upper atmosphere conditions can provide useful data on the rate at which density can change. A long series of Betasonde density measurements can help better define the expected density uncertainty where a given model atmosphere is used.

The conclusions relating to the Low-background Betasonde flight can be summarized as:

i) The Betasonde operated properly during the entire parachute flight, from 65 km to below 5 km. The only data loss was from some TM dropout at 20-24 km.

ii) The reduced data above 30 km agree quite well with the mid-latitude Spring/Fall model atmosphere.

iii) The suitability of the Betasonde for making upper atmosphere air density measurements has been well demonstrated.

In accord with the above discussion, the following recommendations are made:

i) A program of Low-background Betasonde flights should be continued to provide data on the accuracy of atmosphere models and the expected variations.

ii) A number of Betasonde flight series should be made during periods of rapid upper atmosphere density changes to measure the rate at which air densities can change under extreme conditions.

iii) Development of an on-board solid-state recorder should be carried out in order to eliminate the need for TM, improve the data recover probability, and considerably decrease the complexity of the overall determination of a density profile.

4.2 UV Spectrophotometer

The UV spectrophotometer operated successfully on the Stratcom VI-A balloon flight, and returned much good data on stratospheric solar UV fluxes. The dependence of the solar UV fluxes on solar zenith angle at 30-40 km was measured, and the vertical profile to below 20 km was measured during the parachute descent. One of the few reliable measurements of solar UV in the important high altitude 220 nm atmospheric window was made, giving a solar flux of 3.93×10^{-6} W/(cm^2-nm) (at 220 nm) at 1 AU during solar minimum (Rz= 0). Comparison with other measurements shows a trend of increasing solar flux at 220 nm with increasing solar activity (Rz - sunspot number).

The UVS gave a considerable amount of data on solar UV flux vs. zenith angle for the Sept. 24-25 sunset period. The two sunrise data sets are more sparse because of the warm-up requirement for the solar pointing mechanism. It is planned to eliminate this problem on future balloon flights by using a conical diffuser (see Ref. 1.7) and mounting the UVS in a vertical position. This eliminates the requirement for solar pointing, and thus any problems associated with the pointing mechanism.

During portions of the flight the UVS temperature was considerably lower than had been predicted by theoretical models. Althcugh the UVS continued to operate properly, it was necessary to include small temperature-induced gain shifts into the data reduction procedure to obtain maximum accuracy. It would be desirable to use the UVS internal heaters to avoid this problem if sufficient power were available on future flights.

Since the UVS operated quite satisfactorily and returned a considerable amount of good data, it is recommended that the instrument be flown as frequently as possible over the next several years. Such future balloon flights would use the UVS with a conical diffuser to improve data acquisition during sunrise and parachute descent. Measurements over the 280-400 nm region would be used to monitor the high altitude part of the ozone layer, and provide flux measurements necessary for photochemical calculations. Measurements in the 220 nm atmospheric window would provide important data on the magnitude of solar UV variability in this very important wavelength region. 220 nm solar flux measurements during the rise to solar maximum would help determine if this solar flux depends only on the instantaneous (daily) Rz or the 27 day solar rotation average of Rz, and possibly solar flare influences. The measured altitude dependence would be particularly useful in checking model calculations of UV flux transport in the atmosphere.

Considering the importance of the 220 nm flux to high altitude photochemistry, such measurements are of considerable significance.

The conclusions pertaining to the UVS flight on Stratcom VI-A can be summarized as follows:

i) The UVS operated properly during the entire flight.

ii) Much sunset data were obtained, but sunrise data were less complete because of a warm-up requirement for the sun pointing mechanism.

iii) An absolute measurement of the solar 220 nm flux was obtained. This is in agreement with other measurements, and all together suggest some solar variability at this wavelength.

iv) Vertical UV flux profiles were obtained during the parachute descent, although a significant portion of the data were lost due to instability of the pointing platform at high altitudes during parachute descent.

In accord with the above discussion, the following recommendations are made:

i) On future flights the UVS should be flown with a conical diffuser and pointed vertical, to eliminate data loss from the warm-up requirement of the solar pointing mechanism. The internal heaters should be used, if possible, in order to minimize temperature-induced gain shifts.

ii) The UVS should be flown as frequently as possible during the present rise to solar cycle maximum. This would allow measurement of:

a) 280-400 nm solar fluxes and possible solar cycle related changes in the high altitude part of the ozone layer.

b) 220 nm fluxes to determine more precisely the variation with solar activity and altitude of this important wavelength region.

REFERENCES

1.1 B. Sellers, H. N. Ballard, and M. Izquierdo, Direct Measurement of Air Density in the 30-60 km Region by Beta-Ray Forward Scattering, Intern. J. Appl. Radiation Isotopes 20, 341-51 (1969).

1.2 H. R. Carrasco, Betasonde - High Altitude Mass Density Measurement, Report SR3-75-UA-15, for Contract DAAD07-74-C-0263, The University of Texas at El Paso (May 1, 1975).

1.3 H. N. Ballard, M. Izquierdo, J. Smith, and J. Whitacre, Corrections to Observed Beta-Ray Atmospheric Densitometer Values as Caused by Cosmic Rays, J. Appl. Meteor. 9, 933-9 (1970).

1.4 B. Sellers and F. A. Hanser, Comments on Corrections to Betasonde Density Data Obtained at High Altitudes, J. Appl. Meteor. 11, 880-1 (1972).

1.5 H. N. Ballard, M. Izquierdo, J. Smith, and J. Whitacre, Reply, J. Appl. Meteor. 11, 881-3 (1972).

1.6 R. J. Massa, F. Ostherr, and R. Penndorf, U.S. Department of Transportation CIAP Atmospheric Monitoring and Experiments - The Program and Results, Report DOT-TST-75-106, Final Report for Contract DOT-OS-20104 (June 1975). Available from NTIS, Springfield, Va.

1.7 F. A. Hanser, B. Sellers and J. L. Hunerwadel, Design, Fabrication and Flight of a UV Spectrophotometer Aboard a WB57F High Altitude Aircraft for the CIAP Flight Series, Report PANA-UVS-7, Summary Report for Contract No. N00014-73-C-0316 (December, 1975).

1.8 F. S. Rowland and M. J. Molina, Chlorofluoromethanes in the Environment, Rev. Geophys. Space Phys. 13, 1-35 (1975).

1.9 R. Tousey, The Radiation from the Sun, in A. E. S. Green, ed., The Middle Ultraviolet: Its Science and Technology, 1-39, Wiley, New York (1966).

1.10 A. W. Brewer and A. W. Wilson, Measurements of Solar Ultraviolet Radiation in the Stratosphere, Quart. J. Roy. Meteor. Soc. 91, 452-61 (1965).

REFERENCES (cont'd)

1.11 G. C. Tisone, Measurements of the Absorption of Solar Radiation by O_2 and O_3 in the 2150-A Region, J. Geophys. Res. 77, 2971-4 (1972).

1.12 D. F. Heath, Space Observations of the Variability of Solar Irradiance in the Near and Far Ultraviolet, J. Geophys. Res. 78, 2779 (1973).

2.1 U. S. Standard Atmosphere Supplements, 1966, U. S. Government Printing Office, Washington, D. C. (1966).

2.2 R. D. Evans, The Atomic Nucleus, McGraw-Hill, New York (1955).

3.1 B. Sellers, F. A. Hanser, and J. L. Hunerwadel, Design, Fabrication and Flight of an Ultraviolet Interference-Filter Spectrophotometer Aboard a WB57F High Altitude Aircraft, Report PANA-UVS-1, Annual Report for Contract No. N00014-73-C-0316 (October 1973).

3.2 F. A. Hanser and B. Sellers, Solar UV Fluxes and Ozone Overburdens Obtained from UVS Measurements on the CIAP Airstream Flight Series of June 1973, September 1973, November 1973, and January 1974, Report PANA-UVS-4, Annual Report for Contract No. N00014-73-C-0316 (August 1974).

3.3 The American Ephemeris and Nautical Almanac for the year 1975, U. S. Government Printing Office, Washington D. C. (1973).

3.4 Solar-Geophysical Data, issued monthly by U. S. Dept. of Commerce, NOAA, Environmental Data Service, Boulder, Colorado.

3.5 P. Simon, Balloon Measurements of Solar Fluxes between 1960Å and 2300Å, in Proceedings of the Third Conference on the Climatic Impact Assessment Program, A. J. Broderick and T. M. Hard, Editors, DOT-TSC-OST-74-15,137 (November 1974).

3.6 M. Ackerman, D. Frimout, and R. Pastiels, New Ultraviolet Solar Flux Measurements at 2000Å using a Balloon Borne Instrument, in New Techniques in Space Astronomy, Labuhn and Lust, eds., 251, Reidel, Dordrecht, Holland (1971).

3.7 A. L. Broadfoot, The Solar Spectrum 2100-3200Å, in Astrophys. J. 173, 681 (1972).